npj | clean water

Article

Published in partnership with King Fahd University of Petroleum & Minerals

https://doi.org/10.1038/s41545-024-00376-9

S-ZVI@biochar constructs a directed electron transfer channel between dechlorinating bacteria, *Shewanella oneidensis* MR-1 and trichloroethylene

Honghong Lyu[1] ✉, Hua Zhong[1], Zhilian Li[1], Zhiqiang Wang[1], Zhineng Wu[1] ✉ & Jingchun Tang[2] ✉

The combination of micron zero-valent iron (mZVI) and microorganisms is an effective method for trichloroethylene (TCE) degradation, but electron transfer efficiency needs improvement. A new chem-bio hybrid process using a composite material (S-ZVI@biochar) was developed, consisting of sulfurized mZVI and biochar as a chemical remover, and Shewanella oneidensis MR-1 and dechlorinating bacteria (DB) as a biological agent for TCE degradation. S-ZVI@biochar showed improved stability, biocompatibility, and TCE removal compared to ZVI and S-ZVI. The hybrid system DB + MR-1 + S-ZVI@biochar exhibited the highest TCE removal efficiency at 96.5% after 30 days, which was 3.7 times higher than that of bare ZVI. The study revealed that the enhanced dechlorination performance was due to improved electron transfer efficiency, adjustment of microbial community structure, and iron recycling. S-ZVI@biochar constructed electron transport channels in the composite system, improving the overall dechlorination capacity. This system shows promise for long-term TCE removal in anaerobic environments.

Trichloroethylene (TCE) is widely used across various industries. However, TCE is a mutagenic, teratogenic, and carcinogenic substance that threatens human safety. TCE is also a heavy non-aqueous phase liquid (DNAPL) that migrates downward under gravity, so TCE in groundwater is usually in an anoxic or anaerobic environment. Traditional remediation technologies for TCE pollution typically fall under three major categories: physical, chemical, and biological. The chemical method utilizing zero-valent iron (ZVI) has proven simple, fast, and efficient. On the other hand, the biological method involving dechlorinating bacteria (DB) offers a green and low-cost solution. Both strategies show promise for in situ remediation of TCE-contaminated groundwater. ZVI is regarded as a good material for the reduction of TCE due to its high reducing power ($E_0 = -0.44$ V) and the production of non-toxic iron oxide products[1]. The main route of electron transfer is direct transfer, which means that ZVI releases two or three electrons and is converted into Fe(II) or Fe(III), while TCE receives these electrons and gets reduced[2]. For example, it has been demonstrated that ZVI degrades TCE by β-elimination and hydrogenolysis[3,4]. *Dehalococcoides mccartyi* strain 195 was found to be the first *Dehalococcoides* strain capable of completely reducing perchloroethylene (PCE) or TCE to ethylene[5]. As TCE is dechlorinated in the membrane bioreactor, *Dehalococcoides* are enriched in the biofilm community, demonstrating the presence of dechlorinating bacteria (DB) in the autotrophic microbial community[6]. However, both the ZVI system and the dehalogenation microbial system acting alone have the following drawbacks: (1) Although ZVI is highly reactive, it easily reacts with water to produce H_2 to escape. However, this H_2, as a weak electron donor, cannot be effectively used as a reducing agent in the ZVI system. Instead, it accumulates in the porous medium, and the electrons generated by ZVI corrosion are inefficiently utilized by the pollutants directly[7]. In addition, ZVI is prone to agglomerate due to its particle size and magnetic properties, significantly reducing the contact area between ZVI and the target pollutants. Meanwhile, in practical applications, ZVI reacts with substances in the environment (e.g., H_2O, O_2, NO_3^-), resulting in the formation of an oxidized layer that passivates the surface of ZVI[8]. These factors impede electron transfer between ZVI and the surrounding environment, leading to a shorter lifespan for ZVI, and a lack of long-term effectiveness in practical applications. (2) Anaerobic bioremediation based on

[1]Tianjin Key Laboratory of Clean Energy and Pollution Control, School of Energy and Environmental Engineering, Hebei University of Technology, Tianjin, 300401, China. [2]MOE Key Laboratory of Pollution Processes and Environmental Criteria/Tianjin Engineering Research Center of Environmental Diagnosis and Contamination Remediation, College of Environmental Science and Engineering, Nankai University, Tianjin, 300350, China. ✉e-mail: honghonglyu@hebut.edu.cn; wuzhineng524@163.com; tangkjch@nankai.edu.cn

dechlorinating bacteria often lacks electron donors and nutrients to efficiently complete dechlorination. To overcome this limitation, additional injection of exogenous electron donors is required, which presents technical difficulties and high investment requirements. In addition, the bioremediation process is generally time-consuming, which restricts the widespread application of in situ bioremediation[9–13]. Moreover, free microorganisms need to enhance electron transfer in the dechlorination process. For this reason, a combination of chemical and biological dechlorination can be considered to build a system for synergistic dechlorination of materials and microorganisms. However, there are still unresolved challenges in this synergistic system that ZVI agglomerates and passivates easily, and the electron transfer efficiency between materials, microorganisms and pollutants needs to be improved.

Modifying the physicochemical properties of ZVI would have great application value. There are many options for modification of ZVI, including modification using surfactants, elemental doping modification, etc. Surfactants are a class of amphoteric compounds that contain both hydrophilic and lipophilic groups. This property makes it easier for the product to be absorbed by the surface of the metal particles to reduce interfacial energy, which is more suitable for promoting the transfer of substances in the dechlorination process[14]. However, the use of surfactants may block the active sites preventing adsorption and electron transfer between ZVI and contaminants. Elemental doping modifications can be categorized into non-metallic doping and metallic doping based on the class of dopant elements. Non-metallic doping modification usually involves adjusting the electronic structure, surface activity and catalytic activity of ZVI. For example, nitrogen doping can improve the electronic conductivity of ZVI and increase its reducing ability. The presence of nitrogen may alter the surface properties of ZVI and increase its interaction with contaminants[15]. Phosphorus doping may improve the surface properties of ZVI particles and increase their effectiveness in adsorption and catalysis[16]. Sulfur doping improves the catalytic activity of zero-valent iron and induces more efficient degradation of organic pollutants[17]. The altered properties of metal doping are mainly in terms of electronic structure, catalytic activity, corrosion resistance, stability, and surface activity. Although non-metallic elements such as nitrogen and phosphorus have some advantages in ZVI modification, they may also have some disadvantages that may affect their effectiveness in specific applications. Nitrogen doping may sometimes initiate undesired reactions, such as reacting with oxygen in water to form oxides, which may slow down the rate of the reduction reaction of ZVI. In addition, the preparation of nitrogen-doped ZVI may be complex and may require special synthesis methods, increasing the difficulty and cost of preparation. Phosphorus doping may compete with ZVI and affect the reduction reaction of ZVI, which may slow down the degradation rate of pollutants. The presence of phosphorus may alter the surface properties of ZVI and affect its adsorption performance for certain pollutants. Comparatively, sulfur has a higher potential for application in the modification of ZVI by non-metallic elements. Sulfurized ZVI can become an effective material for environmental remediation through enhancing catalytic activity, improving electronic conductivity, enhancing corrosion resistance, and other properties. In ZVI composites doped with high-electrode potential metals (Cu, Pd and Ni, etc.), ZVI and the high-electrode potential metals form a macroscopic protocell, which accelerates the electron transfer on the surface of ZVI, making the pollutants more susceptible to obtaining electrons for reduction reactions[18,19]. However, metal element doping accelerates chemical corrosion and may cause secondary contamination by heavy metal leaching. Therefore, sulfide modification is a relatively more promising method for application[20].

Sulfurization-modified ZVI (S-ZVI) has been considered as an effective modification of ZVI. Sulfurization results in the formation of iron sulfide (Fe_xS_y) on the surface of ZVI, which acts as a good electro-semiconductor compared to iron (hydr)oxides present on the ZVI surface. This enhanced electron transfer ability facilitates the electron transfer from the ZVI core to the electron acceptor[3,21,22]. Moreover, the presence of iron sulfide reduces the rate of ZVI corrosion by water, thereby minimizing unnecessary electron loss. In addition, the hydrophobic nature of iron sulfide on the surface of ZVI enhances its interaction with hydrophobic pollutants, leading to improved selective removal of the pollutants[23–25]. For instance, research has demonstrated the enhanced selective removal of TCE using S-ZVI through sulfurization of ZVI was improved[3]. S-ZVI has been investigated for the dechlorination of TCE[26,27] and other chlorinated organics[22], both independently and as catalysts. However, a major drawback of S-ZVI is its tendency to agglomerate and exhibit poor dispersion in practical applications, which leads to a reduction of reactive active sites and overall utilization efficiency of the material. To overcome this limitation, one possible approach is to combine S-ZVI with biochar with good electrical conductivity by ball milling as the resulting composites exhibit enhanced reactivity and biocompatibility. In a synergistic system involving DB and S-ZVI@biochar, S-ZVI@biochar gradually becomes encapsulated by an oxidized layer, leading to a gradual reduction in reactive sites and hindering the realization of a self-driven synergistic system.

Dissimilated iron-reducing bacteria play a crucial role in the geochemical cycling of iron compounds, which *Shewanella* is widely used in the current study, which can enhance the removal of TCE by ZVI through reactivating the passivated ZVI[28]. Furthermore, *Shewanella* modulates the growth of DB to promote the biological removal of TCE[29]. Biogenic Fe(II) exhibits a dechlorination capacity[30–32] and is converted to Fe(III) while dechlorinating. When MR-1 is added, the recycling of iron in the system can be realized. Additionally, biochar can complex Fe(II) and reduce the accumulation of solid-phase Fe(II) on microorganisms and Fe(III), thereby preventing the accumulation of Fe(II) from hindering the Fe(III) reduction reaction[33]. Therefore, the synergistic system of S-ZVI@biochar and dehalogenating DB, along with the presence of *Shewanella*, has a significant positive impact on the construction of a long-lasting TCE degradation system.

Current research has focused on the modification of ZVI, ZVI coupled with dehalogenating microorganisms, and iron-reducing bacteria coupled with dehalogenating microorganisms to enhance the removal of chlorinated organics[27,34,35]. Comparing the degradation of TCE by CS@ZVI and CS@ZVI + BL5 systems, it was found that the addition of microorganism BL5 increased the degradation rate of TCE from 78.68% to 99.75%[36]. Regarding combined use of mZVI and autotrophic hydrogen bacteria, it was observed that the mZVI and microbial composite system had a higher application potential than mZVI alone, with a removal efficiency of 75% for TCE (20 mg/L) at 20 days. The removal efficiency and removal rate of the composite system were 1.67 and 5.30 times higher than that of mZVI alone, respectively[9]. The combined effects of biochar and microorganisms can enhance the biodegradation of TCE. Biochar not only adsorbs TCE and creates a low-toxicity environment for microorganisms but also promotes the selective colonization of dechlorinating microorganisms. The time for 100% removal of TCE (10 mg/L) was shortened by biochar from 330 h to 150 h[37]. It was shown that nZVI/BC removed approximately 72% of TCE (47.5 mg/L) within 14 days, but removal could reach 100% after 14 days of biostimulation[38]. Iron-reducing microorganisms not only enhance the dechlorination ability of dechlorinating microorganisms but also activate iron-based materials, thereby extending their service life. It has been demonstrated that the synergy of iron-reducing bacteria and dehalogenating microorganisms improves the removal of TCE. When *Shewanella oneidensis* MR-1 was added to a culture containing *Dehalococcoides*, complete TCE dechlorination was shortened from 24 days to 16 days[29]. The degradational efficiency of TCE (30 mg/L) by aged mmZVI synergized with *Shewanella putrefaciens* with iron reduction increases from 33.3% to 56.7%[28]. However, there has been limited research conducted on the aspects of enhanced electron transfer in chemical and biological processes during dehalogenation. Biochar has been introduced to enhance the connection between chemical and biological reactions, but the specific enhancement effects and mechanisms still require further exploration. It is necessary to investigate how the addition of *Shewanella* regulates the transformation of iron in the system, as well as the changes in the microbial community, in order to achieve long-lasting dechlorination in the composite system.

Metagenomic sequencing has emerged as a prominent area of research, offering a wealth of biological information that can provide insights into functional aspects beyond the composition of a species[39,40].

In this study, S-ZVI@biochar was obtained by the composite of S-ZVI and biochar using the ball milling method coupled with dehalogenating microorganisms and *Shewanella oneidensis* MR-1 (MR-1) for the investigation of TCE dechlorination. The removal performance of TCE from water using S-ZVI and S-ZVI@biochar in combination with dehalogenating microorganisms and *Shewanella oneidensis* MR-1 was systematically compared. Then, the removal performance of the system was optimized for economic efficiency by adjusting the dosage of S-ZVI@biochar and the addition of sodium acetate. The objectives of this work were as follows: (1) Exploring the enhanced electron transport capacity and dechlorination of S-ZVI by biochar in S-ZVI@biochar. (2) Speculating on the electron transfer between S-ZVI@biochar, microorganisms, and TCE enhanced by biochar in S-ZVI@biochar. (3) Verifying the long-term remediation of TCE in water through a combination of S-ZVI@biochar, DB, and *Shewanella oneidensis* MR-1 using long-term degradation experiments. This study contributes to the understanding of the coupled dechlorination mechanism between dehalogenating microorganisms, *Shewanella oneidensis* MR-1, and S-ZVI@biochar, providing insights for the design of sustainable remediation programs for practical applications.

Methods

Chemicals

All chemicals used in this study were of analytical grade or higher. The mZVI (400 mesh) was purchased from Chengdu Cologne Chemical Reagent Factory. Trichloroethene (TCE; 99.5%), cis-dichloroethene (cis-DCE; 98%), trans-dichloroethene (trans-DCE; 98%), 1,1-dichloroethene (1,1-DCE; 99%) and vinyl chloride (VC; 99%) were obtained from Kmart (Tianjin) Chemical Technology Co. Sodium dithionite was purchased from Tianjin Damao Chemical Reagent Factory, China, and 2-(N-morpholine) ethanesulfonic acid monohydrate was purchased from Bide Pharmaceutical Co. Deionized water produced by equipment model CM-RO-C2 was used for the preparation of all reagents and particle suspensions. The 2-(N-morpholino) ethanesulfonic acid (MES) buffer solution was configured as follows: 10.6625 g of 2-(N-morpholine) ethanesulfonic acid monohydrate was dissolved in 1 L of deionized water and the pH was adjusted to 6 to obtain the MES solution (50 mM, pH = 6).

Cultivation of microorganisms

The dehalogenation bacteria used in this study were isolated from the soil samples taken from a chemical plant in Binhai New Area, Tianjin, China. To obtain the bacteria, 5 g of soil was soaked in 20 mL of saline solution for 24 h, and 5 mL of the supernatant was taken and transferred to 45 mL of anaerobic medium containing 30 mg/L of TCE. After 15 d of cultivation, 5 mL of the bacterial solution was transferred to another 45 mL of anaerobic medium with 30 mg/L of TCE. This process was repeated three times to obtain the DB, which included *Pseudomonas*, *Delftia*, *Comamonas*, *Paraclostridium*, *Tessaracoccus*, *Stenotrophomonas*, *Paenibacillus*, *Acidovorax*, *Clostrdium*, and *Paeniclostridium*.

The anaerobic medium was prepared with the following reagents per liter[41]: 10 mL of salts solution, 1 mL of Se/W solution, 1 mL of trace element solution, and 0.25 mL of 0.1% (w/v) resazurin stock solution, as described in previous research. Additionally, 2.292 g of N-[Tris(hydroxymethyl) methyl]-2-aminoethanesulfonic acid (TES) was added as a buffer, and 1.87 g of sodium lactate was added as a carbon source and electron donor. The anaerobic medium was then flushed with N_2, boiled for 10 min to remove oxygen, and autoclaved. Furthermore, 0.048 g of $Na_2S{\cdot}9H_2O$ and 0.242 g of L-cysteine were added as reducing agents, and 2.52 g of $NaHCO_3$ was added as a buffer. Finally, 0.0771 g of DL-dithiothreitol was added, and HCl was used to maintain the pH value of the anaerobic medium as neutral. In addition, carbon sources (700 mg/L sodium acetate) and cofactors such as VB_{12} (4 μg/L) were added to the anaerobic medium to promote the growth of DB.

Shewanella oneidensis MR-1 was purchased from Beijing Biobw Biotechnology Co. Ltd. MR-1 was cultured anaerobically overnight to the exponential phase in an LB medium supplemented with 10 g/L NaCl, 5 g/L yeast paste, and 10 g/L tryptophan at 30 °C. When the cells reached the stationary phase, they were collected at 8000 r/min for 5 min and then washed three times using sterilized saline solution to remove any residual LB medium. Finally, the cells were resuspended with sterilized saline solution to obtain a cell suspension for further experiments.

Preparation of S-ZVI@biochar

In this experiment, pine wood chips were used as the raw material for the preparation of biochar. The pine wood chips were washed and dried in a blast drying oven at 80 °C. Subsequently, the dried pine wood chips were placed in a vacuum atmosphere furnace and pyrolyzed to produce biochar. The vacuum atmosphere furnace was evacuated and filled with nitrogen to create an oxygen-free environment. A constant nitrogen flow rate of 500 mL min^{-1} was maintained throughout the atmosphere furnace, and the temperature was increased at a rate of 5 °C min^{-1} from room temperature to 600 °C. The carbonization process was maintained at 600 °C for 2 h. Once the instrument cooled down to room temperature, it was turned off and the biochar was removed for preservation and further use, which was recorded as biochar.

S-ZVI@biochar was prepared by first sulfurizing mZVI with sodium dithionite, followed by the direct ball milling of the sulfurized S-ZVI with biochar. The specific methods were as follows: 1.23 g of mZVI and 190.99 mg of $Na_2S_2O_4$ (S:Fe molar ratio of 1:10) were mixed in a 50 mL centrifuge tube, and 50 mL N_2-purged MES solution (50 mM, pH = 6) was added[42] before the tube was sealed and then spun and mixed on an oscillating mixer for 12 h. After centrifugation of the solution, the solid was washed three times with deionized water and separated by centrifugation at 8000 rpm. The obtained material was freeze-dried in a lyophilizer for 24 h, stored under anaerobic conditions, and named S-ZVI. 1.875 g of S-ZVI and 0.625 g of biochar were added to a stainless-steel milling tank, as well as 3 mm stainless steel balls (250 g). Ball milling at 300 rpm was performed in a nitrogen atmosphere. After 12 h, the material was collected in an anaerobic glove box and stored under anaerobic conditions, and named as S-ZVI@biochar.

Batch experiments

Unless otherwise stated, the DB used was cultured to the logarithmic stage and used in subsequent experiments, 700 mg/L of sodium acetate was added to the different reaction systems, and the TCE level in the system was 10 mg/L. Batch experiments were carried out in 20 mL brown glass vials sealed with aluminum caps with Teflon. In addition to the added microorganisms and TCE, the rest of the reaction system was brought up to 7 mL using the anaerobic medium described above. The dosage of the material was 0.5 g/L in the ZVI, S-ZVI and S-ZVI@biochar systems. In the DB + S-ZVI and DB + S-ZVI@biochar systems, the inoculum of DB was 0.7 mL[29], and the dosage of the material was 0.5 g/L. In the DB + MR-1 + S-ZVI and DB + MR-1 + S-ZVI@biochar systems, the DB was inoculated at 0.7 mL, the material was dosed at 0.5 g/L, and the volumetric ratio of the addition of MR-1 (OD_{600} = 0.1) to the final reaction volume was 1:250[29]. The design of the batch experiments was presented in Table 1. All experiments were performed at 30 °C in the dark. In this work, each experiment was repeated three times, the average value was taken as the result, and the results of the repeated experiments were shown as error bars added to the figures. Sterile anaerobic medium containing 10 mg/L TCE was run as a negative control.

Analytical methods

TCE and related dechlorination products (i.e., cis-DCE, trans-DCE, 1,1-DCE, VC, acetylene, and ethylene) were determined by gas chromatography (GC) and the analytical procedure was as follows. Brown serum vials were heated in the headspace (7697 A, Agilent Technology, USA) at an equilibrium temperature of 80 °C for 30 min. GC-FID (7890B, Agilent Technology, USA) with a GS-Q column of 30 m length and 0.53 mm outer

Table 1 | The constituents of batch experiments

System	TCE (mg/L)	DB (OD_{600} = 2.0) (mL)	MR-1 (OD_{600} = 0.1) (μL)	Materials	
				Type	Dosage (g/L)
DB	10	0.7	×	×	×
DB + MR-1	10	0.7	28	×	×
ZVI	10	×	×	ZVI	0.5
S-ZVI	10	×	×	S-ZVI	0.5
S-ZVI@biochar	10	×	×	S-ZVI@biochar	0.5
DB + S-ZVI	10	0.7	×	S-ZVI	0.5
DB + MR-1 + S-ZVI	10	0.7	28	S-ZVI	0.5
DB + S-ZVI@biochar	10	0.7	×	S-ZVI@biochar	0.5
DB + MR-1 + S-ZVI@biochar	10	0.7	28	S-ZVI@biochar	0.5

diameter and nitrogen carrier gas is used. The inlet temperature was 200 °C, the inlet split ratio was 10:1, the flow rate of carrier gas was 25 mL/min, and the temperature of the FID detector was 230 °C. The column temperature was 50 °C for 7 min, then 20 °C/min until 230 °C, and the column temperature was maintained at 230 °C for 10 min. The injection volume was 1000 μL of gas, and the quantitative analysis of TCE was performed by the external standard method. Concentrations of TCE, DCEs, VC, acetylene, and ethylene were determined by comparison of GC peak areas to a five-point external standard curve. The detection range of TCE was 0.1−10 mg/L.

The concentration of total Fe was determined by Inductively Coupled Plasma Atomic Emission Spectrometry (ICP-AES) (IRIS Intrepid II XSP, Thermo Elemental, Waltham, MA, USA). The concentration of dissolved Fe(II) was measured by the Phenanthroline method (3500B)[43]. H_2 concentration was detected by a gas chromatograph (GC 7900, Shanghai Tianmei Scientific Instrument Co., China) equipped with a thermal conductivity detector. The pH and ORP of the systems were measured using a pH or ORP meter (HQ 11d Portable pH/ORP Meter, Hach Inc., USA). The growth of the bacteria was presented with OD_{600} using a Shimadzu UV-1800 spectrophotometer.

Solid particles were collected after 30 days of the experiment and were freeze-dried for 48 h for subsequent characterization. Field emission scanning electron microscopy (Thermo Scientific K-Alpha, USA) was used to view the morphology and determine the elemental composition. X-ray photoelectron spectroscopy (XPS; K-Alpha, Thermo Fisher Scientific, UK) analysis was conducted with a monochromatic Al Kα X-ray source at 1486.6 eV and XRD diffraction spectroscopy (XRD, Ultima IV, Rigaku) was used to identify mineral components before/after the reaction.

Metagenomic sequencing

Samples of DB before reaction, DB, DB + S-ZVI@biochar and DB + MR-1 + S-ZVI@biochar after 30 days of reaction were taken respectively, and were used to assess the changes in the bacterial community and gene before and after the bioremediation process.

Extraction was performed using the Tengen DP705 kit, Qbiut (Invitrogen, Qubit 3.0, Qubit TM dsDNA HS Assay Kit) was used for concentration testing of the extracted nucleic acids, and agarose electrophoresis was used to test the integrity of the extracted nucleic acids on a 1% agarose gel. PCR amplification reaction conditions: initial 95 °C for 3 min, followed by 9 cycles of 98 °C for 20 s, 60 °C for 15 s, 72 °C for 3 s, and a final extension of 72 °C for 5 min. Purification was performed with Vazyme DNA Clean magnetic beads, which were equilibrated at room temperature for more than 30 min before use.

Library construction was performed with the VAHTS® Universal Plus DNA Library Prep Kit for IIIumina ND617 kit, following the instructions. The libraries were subjected to fragment quality control using Qsep-400, quantification of library concentration using Qubit 3.0, and sequencing of the constructed libraries using the Illumine Novassq 6000 sequencing platform.

Raw reads obtained from sequencing contain low-quality sequences, which need to be filtered to obtain clean reads for subsequent analysis to ensure the quality of the information analyzed. The raw tags were then filtered using fastp software to obtain clean tags. Macrogenome assembly was performed using the software MEGAHIT to filter contig sequences shorter than 300 bp. QUAST software was used to evaluate the assembly results. MetaGeneMark software was employed to identify coding regions in the genome using default parameters. Finally, MMseqs2 software was used to remove redundancy in the data, with the similarity threshold set at 95%, and the coverage threshold set at 90%.

Result and discussions

TCE removal in different reaction systems

It can be seen that the removal efficiency of DB for TCE increased rapidly during the initial and middle periods (Fig. 1), reaching 47.6% and 55.5% at 14 and 30 d, respectively. This might be attributed to the high nutrient content of the system during the first two weeks, which led to the rapid growth of DB and improved dechlorination capacity. However, as TCE was dechlorinated, it produced more toxic dechlorination byproducts that were harmful to DB, ultimately reducing the biological dechlorination of TCE by DB. The ZVI reaction system showed a low removal efficiency, with only 20.6% and 26.0% removal rates at 14 and 30 days, respectively. This was due to the iron oxides on the surface of ZVI, which greatly hindered internal contact with the outside world, while the agglomeration of ZVI largely reduced its reactive active sites. Sulfurization of ZVI enhanced the removal of TCE by the material. The S-ZVI system showed an increase in TCE removal, with rates of 31.0% and 37.8% at 14 and 30 days, respectively. Although S-ZVI was effective in removing TCE, agglomeration could still occur and affect its utilization efficiency. Biochar-modified S-ZVI had a large improvement in TCE removal capacity. In the S-ZVI@biochar system, the removal of TCE showed a rapid increase in the first and middle stages, with a removal rate of 80.8% at 14 days and 88.5% at 30 days. It was found that the dechlorination of DB alone and materials alone was not satisfactory. However, when the DB was combined with the material for 30 days, the DB + S-ZVI system improved the removal efficiency of TCE by 81.4% over the S-ZVI system and the DB + S-ZVI@biochar system improved the removal efficiency of TCE by 5.7% over the S-ZVI@biochar system. This suggested that the synergistic effect of DB with the material has faster removal kinetics.

Although MR-1 was found to have no degradation effect on TCE[29], experimental results revealed that the synergistic effect of DB and MR-1 enhanced the dechlorination of DB. After 30 d of reaction, the addition of MR-1 was found to improve the TCE removal efficiency by 16.3% and 3.2% for DB + S-ZVI system and DB + S-ZVI@biochar, respectively. The final removal efficiency improvement was less, but it is evident that MR-1

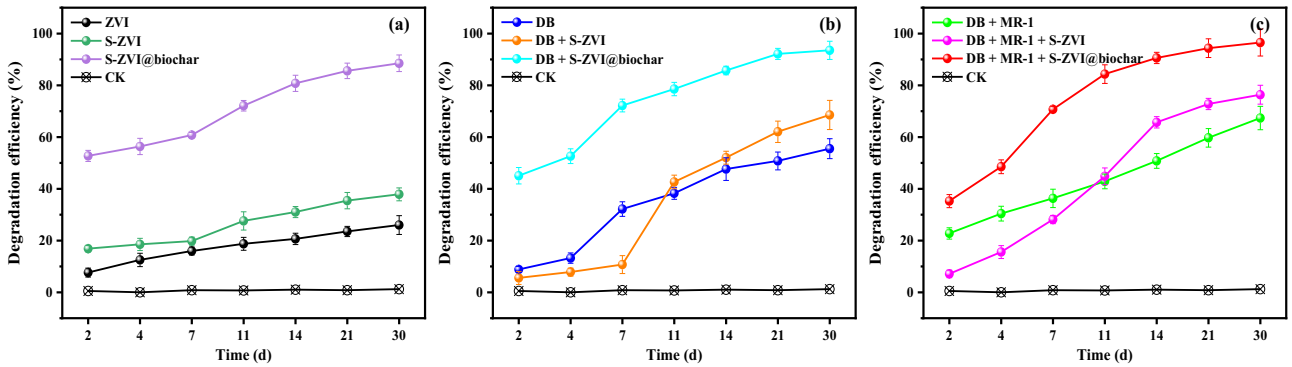

Fig. 1 | Variation in degradation efficiency of TCE at different times in different degradation systems. a Comparison of the effect of modification of materials on their degradation efficiency. It shows that sulfurization modification and biochar modification improve the dechlorination capacity of ZVI. **b** Shows the degradation efficiency of DB alone and DB when synergized with S-ZVI and S-ZVI@biochar, respectively. It shows that DB has better synergistic effect with S-ZVI@biochar. **c** Shows the degradation efficiency of the microbial action of DB + MR-1 and DB + MR-1 in synergistic interaction with S-ZVI and S-ZVI@biochar, respectively. It shows that DB, MR-1, and S-ZVI@biochar have good synergistic ability to degrade TCE.

accelerated the removal of TCE. For example, DB + S-ZVI@biochar took 21 days to reach 92.1% removal efficiency, whereas DB + MR-1 + S-ZVI@-biochar achieved 90.6% in just 14 days. The experimental results demonstrated that S-ZVI@biochar could act as a bridge to construct an electronic channel between DB, MR-1 and TCE, and the combined action of the material and microorganisms improved the removal of TCE.

Variation of H_2, pH, and ORP in different reaction systems

The accumulation of H_2 in different reaction systems was summarized in Fig. 2a1–a3. In the S-ZVI and S-ZVI@biochar systems, the amount of H_2 increased rapidly within 14 d and accounted for about 75.6% and 55.4% of the total residual amount at the end of the experiment, respectively. The loading of S-ZVI with biochar resulted in the effective dispersion of S-ZVI@biochar particles. Furthermore, the biochar demonstrated excellent electron transfer capacity, leading to a higher reactivity of S-ZVI@biochar and a relative increase in hydrogen precipitation reaction.

In this study, there was H_2 production in the DB system, which may be due to the presence of bacteria with hydrogen-producing capacity in DB (Fig. 2a2, a3). The microbial community analysis revealed the presence of *Clostridium*, which can produce hydrogen when exposed to high concentrations of chlorinated organic matter[37,44–46]. However, the accumulation of H_2 decreased after 14 d, possibly due to the change in the microbial community structure as the reaction continued, and the dechlorinating bacteria utilized the H_2 for the biodegradation of TCE. The addition of MR-1 increased the production of H_2 in the pre-mid phase (Fig. 2a2, a3), which might be because the growth of MR-1 consumed the sodium acetate in the solution, leading to a decrease in the pH of the solution (Fig. 2b2, b3), which was more suitable for the growth of hydrogen-producing microorganisms[47,48].

Hydrogenase activity controlling microbial hydrogen production is affected by pH[48]. Increasing pH could enhance the ability of hydrogen-producing bacteria to produce hydrogen during the fermentative hydrogen production process over an appropriate range, but exceeding a certain pH range would result in a decrease in hydrogen production capacity[49]. At the same time, the growth and metabolism of MR-1 might produce nutrients that promote the growth of hydrogen-producing microorganisms[50].

During the experiment, there was a rapid increase in hydrogen levels within 7 d in the DB + S-ZVI, DB + S-ZVI@biochar, DB + MR-1 + S-ZVI and DB + MR-1 + S-ZVI@biochar systems. When the reaction reached 14 days, hydrogen levels rapidly decreased and then gradually increased until the end of the reaction. This might be due to less fluctuation in pH over 7 days and the rapid growth of hydrogen-producing microorganisms on the surface of material, which produced more H_2. In addition, the material reacted with water in a hydrogen precipitation reaction, causing a gradual increase in pH, slowing down the growth of hydrogen-producing microorganisms in the DB, and allowing dehalogenating microorganisms to rapidly consume the H_2 in the system to degrade the TCE within 14 d, which corresponded to the TCE removal trend in Fig. 1a–c. The gradual increase in hydrogen accumulation occurred towards the end of the reaction. This is due to a reduction in TCE as an electron acceptor and a subsequent reduction in the amount of H_2 consumed by microorganisms as an electron donor. The trend of ORP also showed a higher reactivity of S-ZVI@biochar than ZVI and S-ZVI. In general, the coupling of DB, MR-1, and S-ZVI@-biochar demonstrated a greater reduction potential (Fig. 2c1–c3).

Characterization of materials and the formation and evolution of corrosion products

The electrochemical properties of ZVI, S-ZVI, S-ZVI@biochar, and Biochar are shown in Fig. 3. The electron accepting capacity (EAC) of ZVI, S-ZVI, S-ZVI@biochar, and Biochar were 12.25, 14.32, 38.58, and 20.31 mmol e^-/g, and the corresponding electron giving capacities (EDC) were 0.12, 0.39, 0.43, and 0.08 mmol e^-/g, respectively (Fig. 3a, b). The electron transfer capacity (ETC = EAC + EDC; mmol e^-/g) of a material describes its total capacity to accept or donate electrons[51]. Therefore, the EACs of ZVI, S-ZVI, S-ZVI@biochar, and Biochar were 12.37, 14.71, 39.01, and 20.39 mmol e^-/g, respectively. It was observed that S-ZVI@biochar has good electron transfer ability. The cyclic voltammetry (CV) curves indicated that the modified S-ZVI@biochar possessed the redox properties of both S-ZVI and Biochar (Fig. 3c). The galvanostatic charge-discharge (GCD) of ZVI, S-ZVI, S-ZVI@biochar and Biochar were 2.27, 3.45, 4.22, and 3.02 F/g, respectively. It showed that the capacitive performance of S-ZVI@biochar was better than that of ZVI, S-ZVI, and Biochar. Therefore, it can be proved that S-ZVI@biochar has good electrochemical properties.

TCE is a hydrophobic volatile organic compound (VOC) and there are two problems in biodegrading this type of pollutant. The first is the mass transfer of contaminants from the gas phase to the liquid phase, and the second is the low efficiency of microbial extracellular electron transfer. The current effective method to increase the solubility of hydrophobic VOC is the use of surfactants[52]. In addition, the use of electron shuttles improves the efficiency of extracellular electron transfer and thus enhances biodegradation[53].

The outward transfer of electrons from the cell is usually through its extracellular polymers, in which redox mediators are present to transfer electrons to electron acceptors through electron leaps. When an electron shuttle is present, it accelerates the transfer of electrons to electron acceptors[51]. The common electron shuttles are soluble anthraquinone substances[54]. This type of substance is consumptive and can't maintain the role of transferring electrons for a long time. Therefore, insoluble electron shuttles such as biochar have greater potential for application. In the coupled

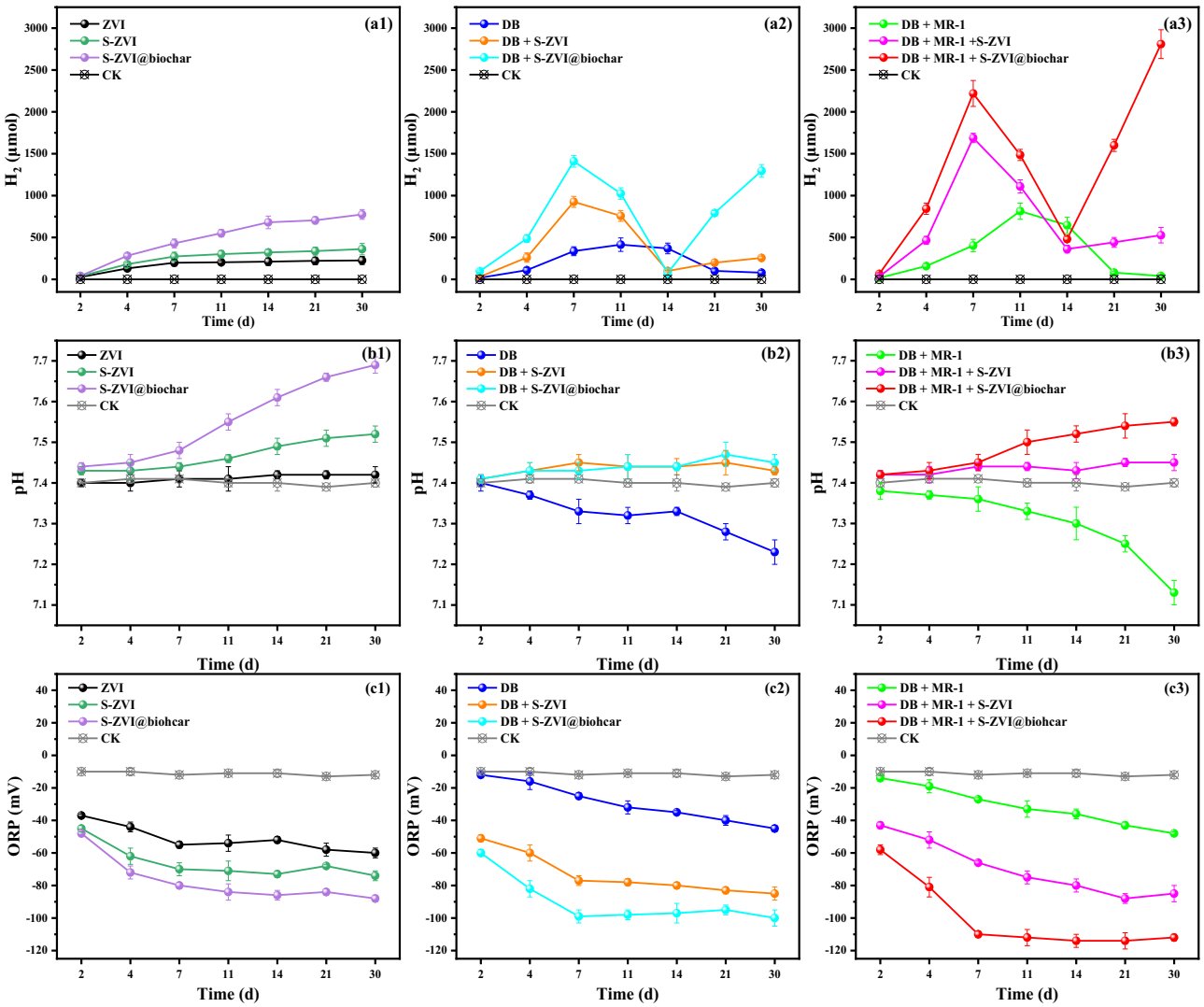

Fig. 2 | Variation of H_2 accumulation, pH, and ORP in different degradation systems. Variation of H_2 accumulation (a), pH (b), and ORP (c) at different times in different degradation systems. a1–c1 Show the variation of H_2 accumulation, pH and ORP in ZVI, S-ZVI, and S-ZVI@biochar systems. It shows that compared to ZVI and S-ZVI, S-ZVI@biochar produces more H_2, increases the pH and decreases the ORP of the system in a greater extent. **a2–c2** Show the variation of H_2 accumulation, pH and ORP in DB, DB + S-ZVI, and DB + S-ZVI@biochar systems. It shows that DB has the ability to produce hydrogen, and S-ZVI and S-ZVI@biochar promote the production of hydrogen by DB. DB decreases the pH of the system, while DB + S-ZVI and DB + S-ZVI@biochar increase the pH of the system. DB decreases the ORP of the system, and DB + S-ZVI and DB + S-ZVI@biochar decrease the ORP of the system further. **a3–c3** Show the variation of H_2 accumulation, pH and ORP in DB + MR-1, DB + MR-1 + S-ZVI, and DB + MR-1 + S-ZVI@biochar systems. It indicates that the presence of MR-1 promotes the H_2 accumulation in the DB + MR-1, DB + MR-1 + S-ZVI,and DB + MR-1 + S-ZVI@biochar systems. Compared to the DB, DB + S-ZVI, and DB + S-ZVI@-biochar systems without MR-1, the presence of MR-1 decreases the pH of the DB + MR-1 system more, while DB + MR-1 + S-ZVI and DB + MR-1 + S-ZVI@biochar increase the pH of the system more. Also, the presence of MR-1 decreases ORP of DB + MR-1, DB + MR-1 + S-ZVI, and DB + MR-1 + S-ZVI@biochar systems further.

system of materials and microorganisms, microorganisms grow on the surface of S-ZVI@biochar and the electron shuttles were in close contact with the extracellular polymers, thereby constructing an electron transport channel. This process made it easier for electrons to hop from the extracellular polymers to the electron shuttles and ultimately to the electron acceptors. The electron transfer channel can enhance the electron transfer of microorganisms. DB can enhance its dechlorination through electron transfer channels, and MR-1 can enhance its iron reduction and produce reduced Fe(II) through electron transfer channels. Furthermore, the electron transfer channel can strengthen chemical dechlorination between S-ZVI@biochar and TCE.

At the beginning of the reaction, Fe(II) was accumulated due to the high reactivity of the material, which constantly produced Fe(II). As the reaction proceeded, the reactivity of the material decreased and the Fe(II) in the solution was constantly consumed, causing the Fe(II) content to initially rise and then fall in the process of the reaction Fig. 4. The solution had an overall alkaline environment, so Fe(III) was mostly in form of solids. A comparison between the S-ZVI@biochar and S-ZVI reaction systems showed that the Fe(II) concentration was lower in the S-ZVI@biochar system during the first and middle stages of reaction than the Fe(II) in the S-ZVI system. This might be due to the negative charge on the biochar surface adsorbing Fe(II). However, as the reaction progressed, the Fe(II) concentration in the S-ZVI@biochar system increased consistently and began to decrease after 21 d, whereas in the S-ZVI system, it continuously decreased after a consistent increase for 14 d. The reason behind this could be the homogeneous dispersion of S-ZVI@biochar and the agglomeration of S-ZVI in the water. As the reaction proceeded, the gradually produced corrosion products encapsulated S-ZVI, reducing the reactive sites. Although Fe(II) from ZVI corrosion could not be utilized by microorganisms as

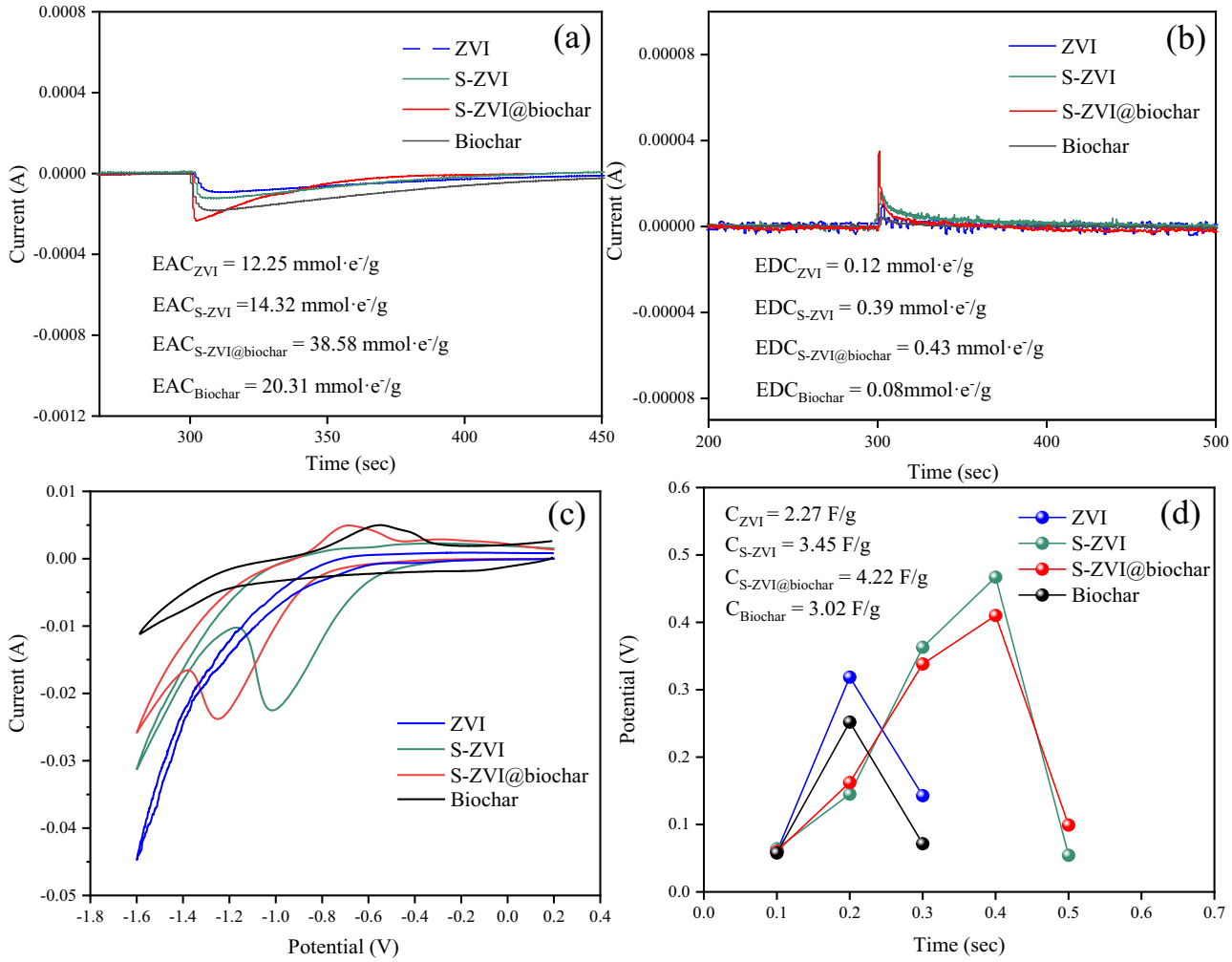

Fig. 3 | Electrochemical characterization of ZVI, S-ZVI, S-ZVI@biochar and Biochar. a EAC of different materials, and it shows that S-ZVI@biochar has the highest EAC. **b** EDC of different materials, and it shows that S-ZVI@biochar has the highest EDC. **c** Cyclic voltammetry characteristic curve, and it shows that the modified S-ZVI@biochar has good electron transfer ability. **d** GCD of different materials, and it shows that S-ZVI@biochar has the highest GCD.

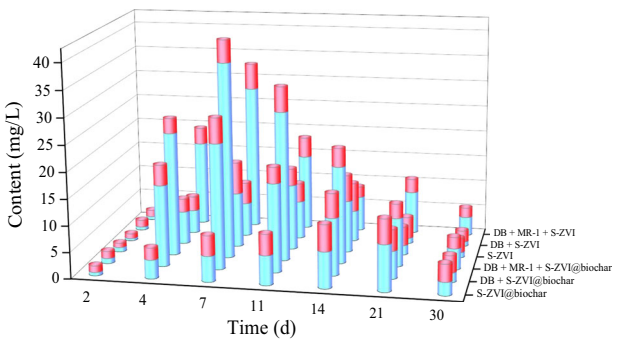

Fig. 4 | Variation of Fe(II) and Fe(III) in solution in different reaction systems. It shows that S-ZVI@biochar has a better ability to consistently produce Fe(II) than S-ZVI. The total content of dissolved Fe(II) and Fe(III) in the microbial-material coupling system shows an increasing and then decreasing trend, and the turnaround time is 7 days. Compared to DB + S-ZVI system and DB + S-ZVI@biochar system without MR-1, the presence of MR-1 increases the dissolved Fe(II) content in the DB + MR-1 + S-ZVI system and DB + MR-1 + S-ZVI@biochar system.

an electron donor, it could still be used as an inorganic nutrient to promote microbial growth[55].

Comparing S-ZVI@biochar, DB + S-ZVI@biochar, and DB + MR-1 + S-ZVI@biochar, it was observed that DB had a promoting effect on the corrosion of S-ZVI@biochar, which might be that DB directly or indirectly utilized the electrons generated by the corrosion of S-ZVI@-biochar. Meanwhile, the addition of MR-1 increased the amount of Fe(II) in the system, which was attributed to the fact that the addition of MR-1 not only affected the community structure of DB but also converted Fe(III) into Fe(II) by its action. As a result, the reduction potential of the system was increased, which also coincided with TCE removal efficiency.

The different morphological structures of S-ZVI@biochar before/after 30 days of reaction, DB + S-ZVI@biochar reaction for 30 d, and DB + MR-1 + S-ZVI@biochar reaction for 30 d are shown in Fig. 5. It was observed that S-ZVI existed in the form of spherical particles and their distribution was relatively uniform, with large gaps between them and no agglomeration (Fig. 5a), which indicated that the poor dispersion of S-ZVI was improved after using biochar as a carrier. Due to its high density, S-ZVI was deposited at the bottom of the culture flasks and clumped together during resting (Supplementary Fig. 4a), which greatly reduced the reactive active sites of S-ZVI and its efficiency. Since biochar is loose, porous and less dense, S-ZVI@biochar was less dense than S-ZVI and was mostly suspended in the solution of the reaction system (Supplementary Fig. 4d). During in-situ remediation, S-ZVI tends to settle at the bottom of groundwater, reducing its migration performance. In contrast, S-ZVI@biochar can migrate with groundwater flow, increasing the scope of groundwater remediation.

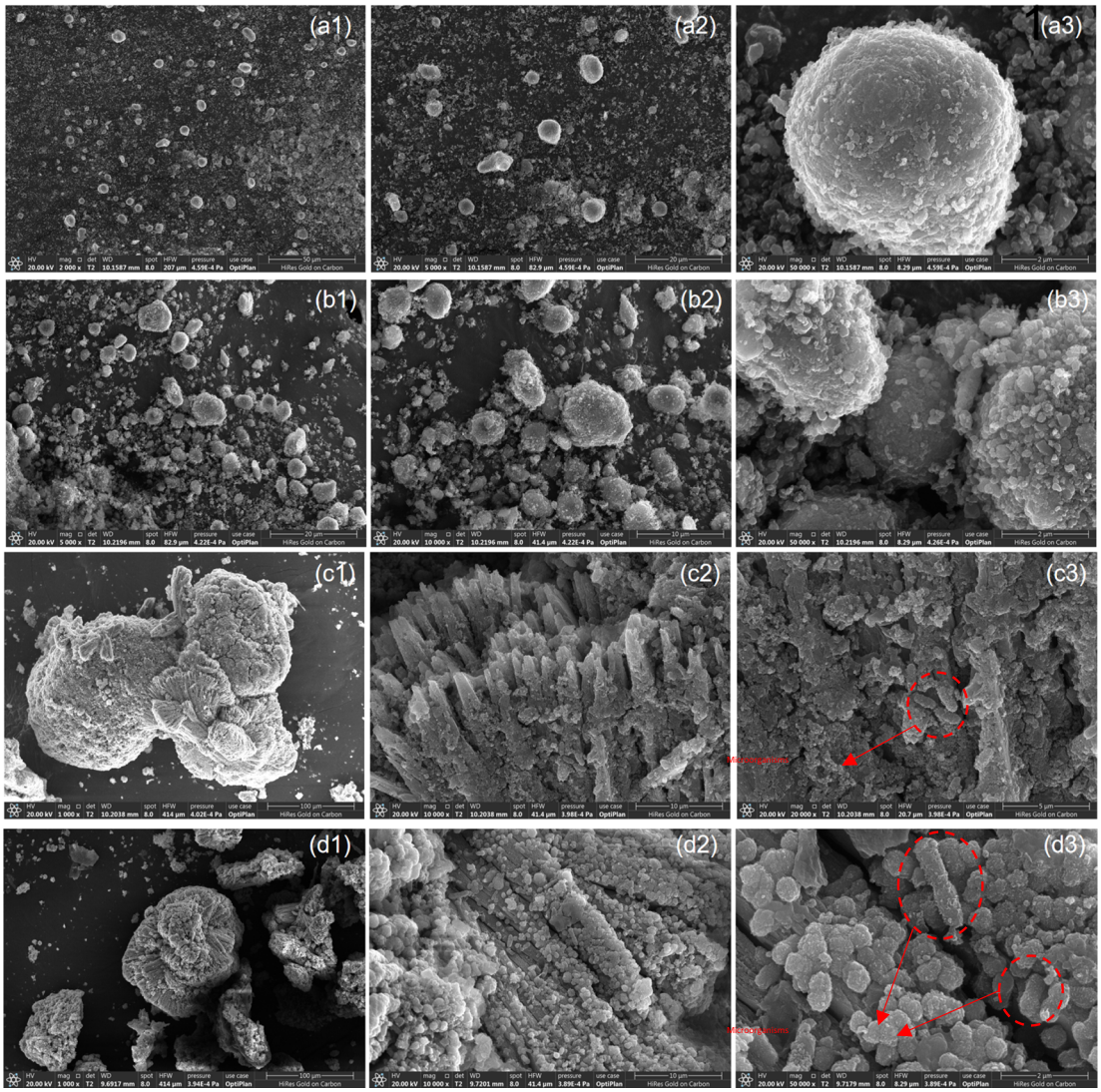

Fig. 5 | SEM images of the materials before and after the reaction. a S-ZVI@-biochar before reaction, and it shows that S-ZVI@biochar has good dispersibility. **b** S-ZVI@biochar for 30 d of reaction, and it shows that the surface of S-ZVI@-biochar produces corrosion products leading to roughness, but still presents a dispersed state. **c** DB + S-ZVI@biochar for 30 days of reaction, and it shows that the structure of corrosion products on the surface of S-ZVI@biochar is changed, while DB grows on the surface of S-ZVI@biochar. **d** DB + MR-1 + S-ZVI@-biochar for 30 days of reaction, and it shows that the presence of MR-1 results in more spherical particles on the surface of the corrosion products of S-ZVI@biochar.

Comparing Fig. 5a, b, it can be observed that the surface of S-ZVI in the reacted S-ZVI@biochar appears to be rougher with some agglomeration, which was attributed to the continuous production and accumulation of iron oxides on the surface of S-ZVI during the reaction process of S-ZVI@biochar with water and TCE in the system. After the addition of DB, it can be seen that the reacted S-ZVI@biochar occurs an obvious agglomeration phenomenon, while a large number of blocks with concentric layers and radial fiber structures can be observed on the surface, which has been verified as acicular ferrite by XRD (Fig. 6c1, c2). This might be due to the growth of microorganisms on the S-ZVI@biochar surface (Fig. 6c3). The electrons that were generated by the corrosion of S-ZVI@biochar were transferred via biochar to the microorganisms, which were then utilized by the microorganisms for the dechlorination of TCE. As a result of the microorganisms' vital activities, the corrosion of mZVI was promoted. By comparing Fig. 5c, d, it was found that after the addition of MR-1, more spherical particles were produced on the surface of S-ZVI@biochar, which were identified as pyrite through XRD analysis (Fig. 6c).

The success of in-situ remediation of the TCE-contaminated groundwater using modified zero-valent iron materials and microorganisms depends on how these materials and dechlorinating microorganisms migrate and distribute in the groundwater. There were differences in their distribution in water, as shown in Supplementary Fig. 4b, c. S-ZVI tends to settle at the bottom of the groundwater and has limited mobility, while microorganisms remain suspended in the groundwater and have a stronger migration capacity. In the actual remediation of groundwater, flowing groundwater amplifies the disadvantage of synergistic action between materials and microorganisms due to the impediment of differences in mobility, which limits their contact and weakens the process of material exchange.

Biochar contains a large number of nanoscale and microscale pore structures[56,57]. Nanoscale micropores not only give biochar a large surface area, but also play an important role in physically adsorbing small molecules[58]. And micron-scale macropores could provide the right-sized habitats for microbiota. In addition, biochar is rich in oxygen-containing reactive groups, which can affect the reduction of pollutants by functional microorganisms. The S-ZVI@biochar material takes advantage of biochar's attachment sites for microbial growth and reduces the distance between S-ZVI@biochar and microorganisms, facilitating their interaction. The electrons generated by S-ZVI@biochar were transferred to microorganisms by means of direct or indirect contact, which increased the electron efficiency in

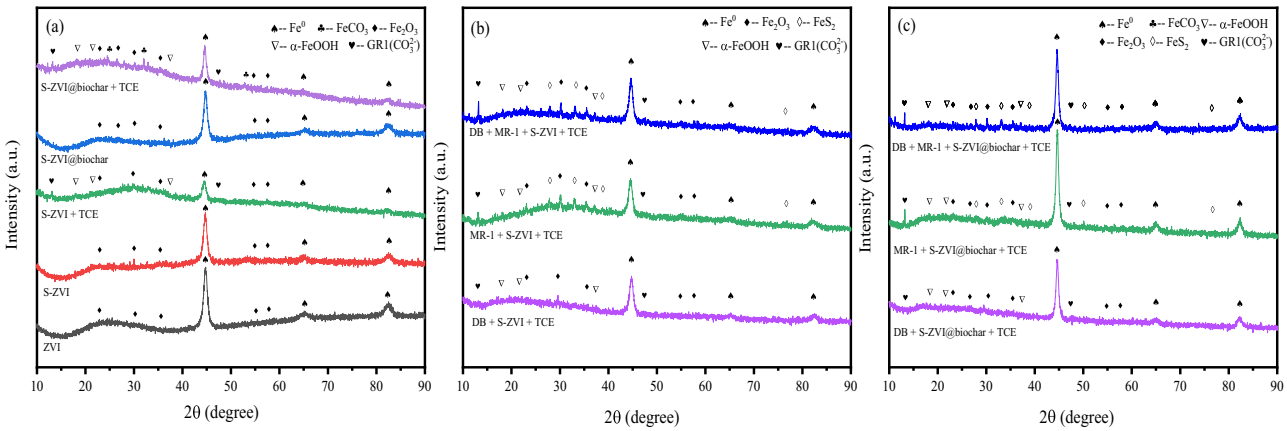

Fig. 6 | XRD of the materials before and after the reaction. a XRD of the different materials before the reaction and after the reaction with TCE alone. After participation in the reaction the Fe^0 signals of both S-ZVI and S-ZVI@biochar are weakened. **b** XRD of the solid-phase material after the S-ZVI co-operative microbial reaction. **c** XRD of the solid-phase material after the S-ZVI@biochar co-operative microbial reaction. The presence of MR-1 promotes the production of GR1(CO_3^{2-}) while exposing more Fe^0.

the reaction system. Microbial growth on the surface of the material improved the co-migration between the material and the microorganism.

As shown in Supplementary Figs. 3c, 4e, f, microorganisms grew on the surface of S-ZVI@biochar in flocculent growth with a high degree of incorporation both in the anaerobic medium and LB medium. This suggested that the addition of biochar increased the potential for synergistic interaction between materials and microorganisms in practical applications.

From the comparison of unreacted S-ZVI and ZVI in Fig. 6a, it was found that the diffraction peaks of Fe_2O_3 of S-ZVI tend to disappear, while the diffraction peaks of Fe^0 were enhanced, which suggested that the antioxidant property of S-ZVI was enhanced compared to that of ZVI, which was due to the role of the sulfide ferrite that covers the surface of Fe^0. Comparing S-ZVI and S-ZVI@biochar before and after the reaction, the diffraction peaks of Fe^0 after the reaction of S-ZVI were significantly weakened, while the diffraction peaks of Fe^0 after the reaction of S-ZVI@biochar were relatively less weakened, which implied that the antioxidant property of S-ZVI@biochar loaded with biochar was higher than that of S-ZVI[59,60]. After the reaction of S-ZVI and S-ZVI@biochar with TCE, S-ZVI@biochar generated more corrosion products, which demonstrated that S-ZVI@biochar was more reactive. Both S-ZVI and S-ZVI@biochar reactions produced green rust and acicular ferrite, which was consistent with previous findings[28].

After the reaction with TCE, the material in the DB + S-ZVI system retained more Fe^0 than the material in the S-ZVI system (Fig. 6b), which might be because when microorganisms were added to the reaction system, they grew and multiplied rapidly to form biofilm on the surface of S-ZVI, which reduced the reactive active sites of S-ZVI and preserved the Fe^0. Moreover, the addition of MR-1 increased the amount of Fe(II) in the reaction system, which was evident in the increase of green rust and FeS_2 content in both the DB + MR-1 + S-ZVI + TCE system and the MR-1 + S-ZVI + TCE system.

The addition of MR-1 increased the amount of Fe(III) on the surface of the solid-phase material after the reaction, comparing the DB + S-ZVI + TCE system and the S-ZVI + TCE system. This increase may be attributed to the fact that MR-1 converted the dissolved Fe(III) in the solution into biogenic Fe(II) with dechlorination ability[61]. Then, the biogenic Fe(II) provided electrons to the contaminants for dechlorination, which transformed into Fe(III) and attached to the surface of the material, so that enhanced diffraction peaks of Fe_2O_3 and α-FeOOH could be observed. It's worth mentioning that under the effect of iron reduction by MR-1, the diffraction peak of FeS_2 was enhanced and the diffraction peak of green rust was weakened. This indicated that the species of biogenic Fe(II) is mainly FeS_2, which was consistent with the SEM plot situation (Fig. 5).

Studies have shown that Fe(II) bound to the surface of iron minerals has a greater reducing ability than that of dissolved Fe(II)[62]. This is because surface hydroxyl groups can act as ligands, forming internal bonds and increasing the electron density around the Fe(II) centers. Additionally, adsorption of multiple Fe(II) atoms in close proximity promotes multi-electron transfer reactions in dechlorination[63]. This corresponded to an increase in the removal efficiency of TCE after the addition of MR-1.

In the C1s orbital of XPS, the most prominent peak at 285.1 eV was for the C-C bond, and the peaks for C-O and C = O bonds were at 286.5 and 288.9 eV, respectively[64]. In the Fe2p orbitals of XPS, at 706.8 and 719.8 eV belonged to Fe^0[65], 709.2, 714.18, and 723.5 eV corresponded to Fe(II)[9], and 711.2, 717.5, and 725.8 corresponded to Fe(III)[66–68]. In the O1s orbitals of XPS, 529.94, 530.73, and 531.97 eV corresponded to Fe-O, O^{2-}, and Fe-OH, respectively[69].

It can be observed that before the reaction of S-ZVI@biochar, the percentage of C-C bonds on the surface was high (Fig. 7a2–d2), which was due to the breaking of some of the biochar particles during ball milling in the preparation process, which then covered the surface of the material. However, during the reaction, the broken biochar particles on the surface of S-ZVI@biochar were dispersed into the solution while the internal S-ZVI@biochar continued to act.

The contents of C = O in Fig. 7b2–d2 accounted for 58.9%, 37.9%, and 41.9% of Fig. 7a2, respectively, and it was observed that the content of C = O in S-ZVI@biochar decreased to varying degrees after the reaction. This might be due to the fact that biochar served as an electron transfer agent between chemical and microbial reactions, and the oxygen-containing functional groups such as quinone and carboxyl groups on the surface of S-ZVI@biochar were depleted[64,70]. When S-ZVI@biochar and DB worked together, it was observed that the oxygen-containing functional groups on the surface of S-ZVI@biochar were consumed to a greater extent. This suggested that biochar played a crucial role in facilitating electron transfer between S-ZVI@biochar, DB, and TCE.

The oxygen-containing functional groups of biochar played an important role in the electron transfer process. For example, the reversible redox reaction between quinone and hydroquinone allowed for the transfer of electrons without requiring additional oxidizing or reducing agents. The reduction of quinone involved the transfer of two electrons. To illustrate, p-quinone can be reduced by accepting one electron to form a p-semiquinone radical as an intermediate and then gaining another electron and two protons for complete reduction to hydroquinone. Conversely, the oxidation of hydroquinone results in the loss of two electrons and two protons[70]. Thus, electrons could be captured and stored by quinone and hydroquinone and released to reduce the target compounds.

The Fe(II)/Fe(III) ratios in Fig. 7a3–d3 were 0.6097, 0.5466, 0.4782, and 0.6690, respectively. As S-ZVI@biochar degraded TCE the ZVI was consumed, which produced more Fe(II) and Fe(III). However, the Fe(II)/Fe(III) ratio decreased from 0.6097 to 0.5466, indicating that some Fe(II)

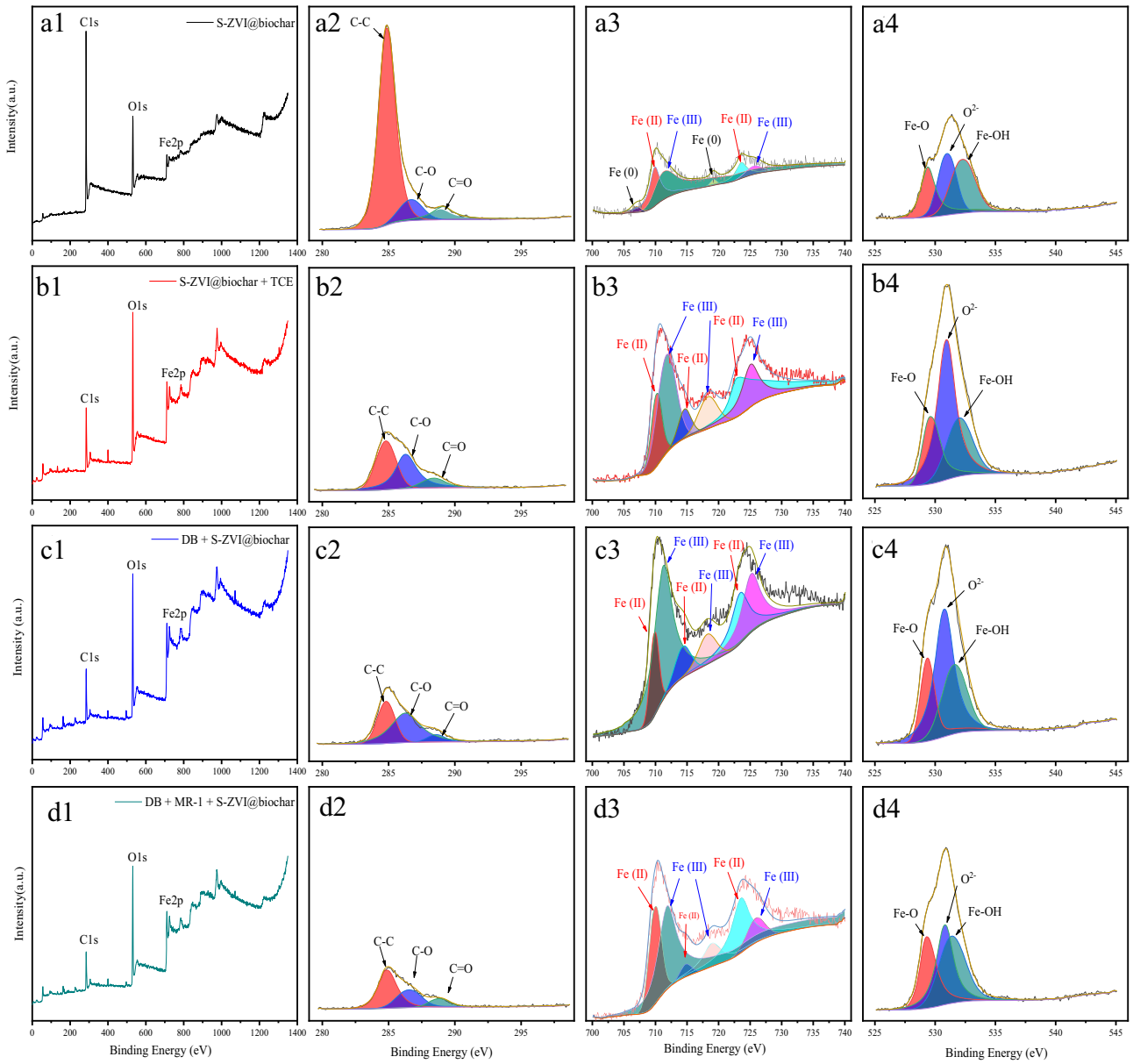

Fig. 7 | XPS spectra of CMC-FeS@biochar before and after TCE reaction in different degradation systems. a1–d1 XPS peaks of S-ZVI@biochar in the initial S-ZVI@biochar and after 30 d of reaction in the S-ZVI@biochar system, the DB + S-ZVI@biochar system, and the DB + MR-1 + S-ZVI@biochar system. There is a decrease in the content of C = O in S-ZVI@biochar after the reaction of different systems. **a2–d2** Corresponds to the C1s orbital analysis of **a1–d1**. **a3–d3** Corresponds to the Fe2p orbital analysis of **a1–d1**. The presence of MR-1 increases the Fe(II)/Fe(III) ratio on the surface of S-ZVI@biochar after the reaction. **a4–d4** Corresponds to the O1s orbital analysis of (**a1–d1**). The presence of MR-1 reduces the O^{2-}content on the surface of S-ZVI@biochar after the reaction.

transformed to Fe(III) after participating in reductive dechlorination. The addition of DB increased the total amount of iron corrosion products because the biochar in S-ZVI@biochar accelerated the electron transfer between S-ZVI@biochar and DB, and DB received the electrons from S-ZVI@biochar, promoting the corrosion of iron. This corresponded with the trend of Fe(II) and Fe(III) in Fig. 4. where MR-1 bioreduced Fe(III) to Fe(II), and the Fe(II)/Fe(III) ratio in the system increased from 0.4782 to 0.6690. The increase in the elemental percentage of Fe2p on the surface of the material after the addition of MR-1 suggested that MR-1 might have dissolved the Fe(III) on the surface of the S-ZVI@biochar to promote the further reaction of the internal ZVI[71].

After the reaction, the O^{2-} percentage increased in both S-ZVI@-biochar and DB + S-ZVI@biochar systems. However, the percentage of O^{2-} decreased significantly after the addition of MR-1. This phenomenon is associated with the production of more FeS_2 and less green rust in the presence of MR-1. Green rust is a class of iron oxides with a complex structure in which oxidizing bonds are formed between iron and oxygen. Specifically, the iron-oxygen bonds in green rust are mainly characterized by chemical bonds between iron ions (Fe^{2+} and Fe^{3+}) and oxygen ions (O^{2-}). These bonds connect the iron ions to the oxygen ions and form the structural unit of green rust[72]. The biological effect of MR-1 was to reduce the lattice oxygen content. Microorganisms have different antioxidant defenses to protect themselves from oxidative damage, including enzymatic and non-enzymatic antioxidants, which neutralized oxidants such as mono-linear oxygen and superoxide anions, thus minimizing oxidative-induced damage[73,74].

Metagenomic sequencing analysis

During the initial stages of the reaction, *Comamonas* was the most predominant genus, followed by *Pseudomonas* and *Delftia* (Fig. 8a). However, after 30 days, the percentage of *Pseudomonas* increased slightly, with *Delftia* becoming the most abundant genus. *Delftia* survived at higher

concentrations of TCE and exhibited dechlorination activity[75,76]. In contrast, *Pseudomonas* showed slow growth when exposed to high TCE concentrations, but effectively dechlorinated the compound at low concentrations[77–79]. This process was employed in conjunction with nZVI to remove TCE, whereby *Pseudomonas* could degrade TCE when nZVI was passivated[80]. Therefore, the proportion of *Delftia* increased dramatically after 30 d of DB reaction and played a major role in dechlorination. When S-ZVI@biochar was added to the system, it reduced the concentration of TCE through physicochemical action, allowing *Pseudomonas* to adapt and grow abundantly. This, in turn, increased the biological dechlorination potential and resulted in further dechlorination[37,81].

This study analyzed the alpha diversity (ACE index, Chao1 index, Shannon index, and Simpson index) of bacterial communities in different systems based on OTU clusters[82]. The results showed that TCE, S-ZVI@biochar, and MR-1 all had a significant effect on the alpha diversity indices of the microbial community in the system (all $p < 0.05$). The results showed that community abundance and diversity in DB decreased after the addition of TCE, indicating that TCE has a toxic effect on microorganisms (Fig. 8b–e). However, after the addition of S-ZVI@biochar, the abundance of microorganisms increased but the community diversity still decreased. According to Fig. 8a, it was observed that *Pseudomonas* became the most dominant genus, which was because the biochar in the material promoted the selective colonization of reductive dechlorinating microorganisms attached to the surface of the biochar. This increased the relative abundance of *Pseudomonas*, while reducing the relative abundance of hydrogen-competing microorganisms, resulting in an efficient reductive dechlorination system[37]. Community abundance further increased after the addition of MR-1 to the system, and community diversity continued to decrease with an increase in the percentage of *Pseudomonas*. This might be due to the fact that the vital activities of MR-1 provided nutrients (e.g., carbon sources and riboflavin) to other microorganisms, promoting the growth of microorganisms with dechlorinating functions[29].

In this study, PCoA, NMDS, and UPGMA analyses were conducted based on a weighted unifrac to reveal the differences in bacterial communities among the systems[83]. The PCoA plot revealed that 93.5% of bacterial community variance was explained by two axes, 74.7% by the first axis and 18.8% by the second axis (Fig. 8f). The closer the samples were to each other, the more similar their species composition was. Overall, the DB system had greater variability before and after the reaction, whereas the DB + S-ZVI@biochar system and the DB + MR-1 + S-ZVI@biochar system had similar community compositions, but they both differed significantly from the DB system. The NMDS plot (stress = 0) showed that bacterial communities in different systems were distinct from each other (Fig. 8g). Furthermore, the UPGMA analysis confirmed the effects of TCE, S-ZVI@biochar, and MR-1 on bacterial communities in different systems (Fig. 8h).

It should be noticed that MR-1 was not observed in the community analysis, which was due to the initial addition of MR-1 being set at a low level to reduce its competitive relationship with DB. Additionally, a certain amount of Fe(III) was reduced to Fe(II) in the system, which suggested that there may be other types of bacteria with iron-reducing functions present in

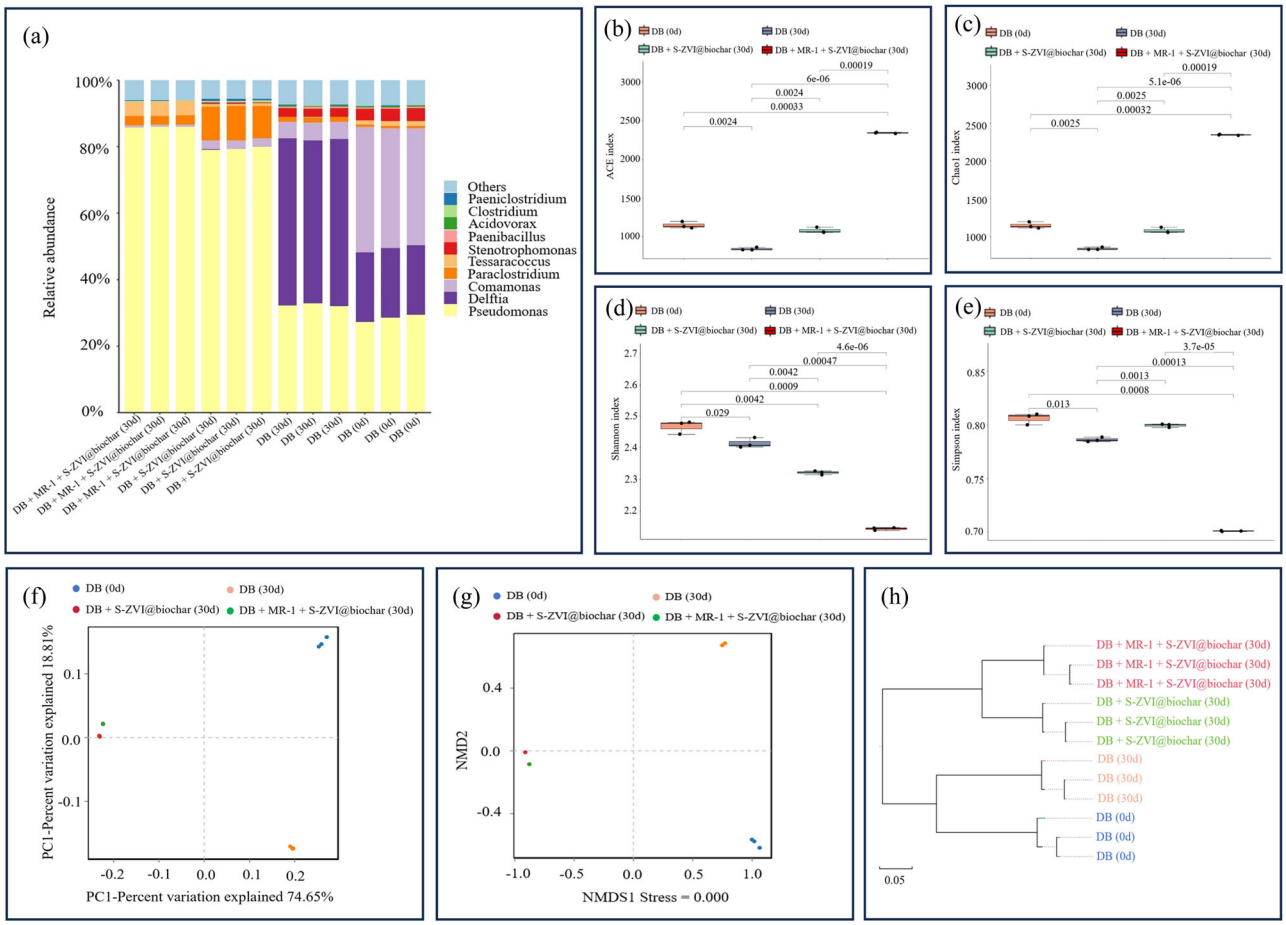

Fig. 8 | Analysis of microbial communities. a Microbial community composition at the genus level. When DB alone reacts with TCE, *Delftia* is the largest percentage of microorganisms in the community. When S-ZVI@biochar is added, *Pseudomonas* becomes the most dominant microorganism in the community in both DB + S-ZVI@biochar system and DB + MR-1 + S-ZVI@biochar system. **b** ACE index of alpha diversity. **c** Chao1 index of alpha diversity. **d** Simpson index of alpha diversity. **e** Shannon index of alpha diversity. **f** PCoA plot of bate diversity. **g** NMDS plot of bate diversity. **h** UPGMA circular tree of bate diversity.

the DB community. Based on the analysis of the community structure at the genus level (Fig. 8a), it can be found that the *Clostridium*, *Paraclostridium*, and *Pseudomonas* present in the community all had the ability of iron reduction[84–86]. In the absence of S-ZVI@biochar, there was no significant change in the percentage of *Clostridium*, *Paraclostridium*, and *Pseudomonas* after 30 d in the DB system. After 30 d of reaction, compared to the DB system, it can be observed that the increase in the percentages of *Clostridium*, *Paraclostridium*, and *Pseudomonas* in the DB + S-ZVI@biochar system were 500.6%, 531.7%, and 145.6%, respectively. And it can be observed that the increase in the percentages of *Clostridium*, *Paraclostridium*, and *Pseudomonas* in the DB + MR-1 + S-ZVI@biochar system were 93.7%, 67.1%, and 165.7%, respectively. The addition of MR-1 decreased the proportion of *Clostridium* and *Paraclostridium* in the community and increased that of *Pseudomonas*. In terms of iron reduction, MR-1, *Clostridium* and *Paraclostridium* were in a competitive relationship. For dechlorination, MR-1 promoted the viability of *Pseudomonas*. This indicated that *Clostridium* and *Paraclostridium* played a major role in iron reduction, while *Pseudomonas* played a major role in dechlorination.

Functional annotation was performed based on KEGG to infer the genetic potential of microbial communities in TCE-containing systems and their adaptive characteristics for the biodegradation of xenobiotic compounds. The predicted enzymes were mapped onto TCE biodegradation pathways to elucidate possible catabolic pathways in the microbial community. As shown in Fig. 9a, the microorganisms within the system have multiple metabolic pathways for degrading TCE and have the potential to completely dechlorinate TCE, which was similar to the results of previous studies[81]. Additional metabolic pathways using different enzymes might cater for the removal of more toxic intermediates, such as cis-1,2-dichloroethene, trans-1,2-dichloroethene, and vinyl-chloride. In addition, the microbial community has a wide range of dechlorination capabilities, and can degrade not only PCE/TCE but also trans-dichloropropene, cis-dichloropropene, 1,1,1-trichloroethane, and other pollutants. This is highly beneficial to the environment and greatly increases the potential for practical application of microbial dechlorination.

It was observed that the percentage of chloroalkane and chloroalkene degradation pathways varied in different reaction systems. Compared to the DB system at 0 days, the increase of relative proportions of chloroalkane and chloroalkene degradation processes to all life processes in the DB, DB + S-ZVI@biochar, and DB + MR-1 + S-ZVI@biochar systems after 30 d of reaction were 4.8%, 13.0%, and 17.6%, respectively. The trend of the change in relative proportions due to the dechlorination process in the different systems was similar to the relative content of *Pseudomonas* in different systems (Fig. 8a), which confirmed that *Pseudomonas* was a major dechlorinator of DB. It indicated that S-ZVI@biochar and MR-1 increased the dechlorination capacity of DB to varying degrees, and the coupling of DB, S-ZVI@biochar and MR-1 was significant.

Dechlorination Mechanisms of DB, MR-1, and S-ZVI@biochar

During the degradation of TCE by the DB system and DB + MR-1 system, the dechlorination products produced were cis-DCE and VC, indicating that hydrogenolysis was the pathway through which TCE was degraded. At a reaction time of 30 days, cis-DCE and VC in the DB system were 10.5 μmol/L and 2.6 μmol/L, respectively, and cis-DCE and VC in the DB + MR-1 system were 14.4 μmol/L and 3.7 μmol/L, respectively. MR-1 could indirectly enhance the role of dehalogenating microorganisms by changing the structure of the microbial community, providing more coenzymes for dehalogenating microorganisms, promoting the secretion of VB_{12} by microorganisms like methanogens, reducing high-valent VB_{12}(III) to low-valent VB_{12}(II), and creating conditions conducive to the reduction of TCE by dehalogenating microorganisms.

During the study, both the S-ZVI system and S-ZVI@biochar system produced ethylene and ethyne as dechlorination products. The process of β-elimination was identified in S-ZVI and S-ZVI@biochar systems. The ethylene and ethyne contents in the S-ZVI system were 2.2 μmol/L and 2.3 μmol/L, respectively, while they were 5.5 μmol/L and 15.7 μmol/L in the S-ZVI@biochar system at 30 days. It was observed that S-ZVI modified by biochar, resulting in S-ZVI@biochar, had higher reactivity and produced more dechlorination products. Comparing the changes of dechlorination products between the S-ZVI system and S-ZVI@biochar system, it was found that S-ZVI@biochar still had dechlorination potential after 21 days, while S-ZVI had almost lost its dechlorination ability after 21 days, which might be due to the fact that S-ZVI was deposited at the bottom of the culture flasks, and the number of reactive sites of S-ZVI were greatly reduced. Iron corrosion products also accumulated on the surface of S-ZVI, which prevented electron transfer between internal Fe^0 and the outside world. In contrast, the biochar in S-ZVI@biochar increased the dispersion of S-ZVI@biochar and reduced aggregation, which coincided with the actual reactions in Supplementary Fig. 4a, d. Furthermore, biochar served as an electron shuttle, facilitating the electron transfer between S-ZVI@biochar and the outside world, which improved the reactivity and service life of the material.

The total amount of ethylene and ethyne produced by the S-ZVI system was higher than that produced by the DB + S-ZVI system (Fig. 10c, d), which indicated that the addition of microorganisms prevented the dechlorination performance of S-ZVI. Similarly, the dechlorination capacity of S-ZVI@biochar was found to be influenced by microorganisms. This might be due to the microorganisms adhering to the surface of S-ZVI, reducing its contact with the outside world. At the same time, the total amount of cis-DCE and VC in the DB + S-ZVI system and DB + MR-1 + S-ZVI system was lower than that in the DB system and DB + MR-1 system, which indicated that S-ZVI also hurt microbial dechlorination ability.

S-ZVI had a typical core-shell structure consisting of Fe^0 as the core center and Fe_xS_y as the outer shell structure, and both of them had complementary or synergistic effects on the removal of pollutants[87]. The structure Fe(II) in Fe_xS_y is an important active substance that oxidizes and removes a wide range of organic and inorganic pollutants in the environment. However, it also has toxic effects on microorganisms by influencing cell growth and metabolic functions[88].

However, the adsorption effect of biochar reduces the spatial distance between S-ZVI, microorganisms, and TCE, which indirectly enhances the transfer of substance between them. In addition, biochar has surface functional groups[89,90] and a graphite-like structure[91,92], which gives it good electrical conductivity. During the dechlorination process of S-ZVI@biochar, the generated corrosion products accumulated on the surface of S-ZVI, hindering the electron transfer between S-ZVI and TCE. However, at the interface of S-ZVI in contact with biochar, biochar could directly promote the electron transfer between S-ZVI and TCE, increasing the S-ZVI@biochar efficiency. It is worth mentioning that the VC/cis-DCE ratios in the DB + S-ZVI@biochar system and DB + MR-1 + S-ZVI@biochar system was higher than those in the DB system and DB + MR-1 system, indicating that microbial dechlorination was enhanced, which was attributed to the biochar in S-ZVI@biochar. The pore structure of biochar provides an ideal environment for microbial growth by offering space and protection[93]. Additionally, biochar contains nutrients and energy that microorganisms require to thrive, while also reducing the growth inhibition caused by interspecific competition between different species, and significantly influenced the composition and activity of microbial communities[64,94]. Moreover, biochar decreased the toxicity of S-ZVI to microorganisms. At the same time, biochar acted as an electron shuttle to transfer electrons from the bacterial surface to halogenated organic matter, accelerating biological dehalogenation[95,96]. Thus, biochar can increase microbial dechlorination[97]. In addition to transferring electrons between microorganisms and contaminants, biochar also strengthened the connection between microorganisms and materials. For instance, biochar can transfer electrons generated by S-ZVI@biochar to microorganisms, which can then be used by DB for bioreductive dechlorination[98]. Moreover, MR-1 can utilize the electrons generated by S-ZVI@biochar to reduce Fe(III) in the system to biogenic Fe(II). This leads to an improvement in the practical efficiency of the electrons produced during the reaction. The Fe(II) was then

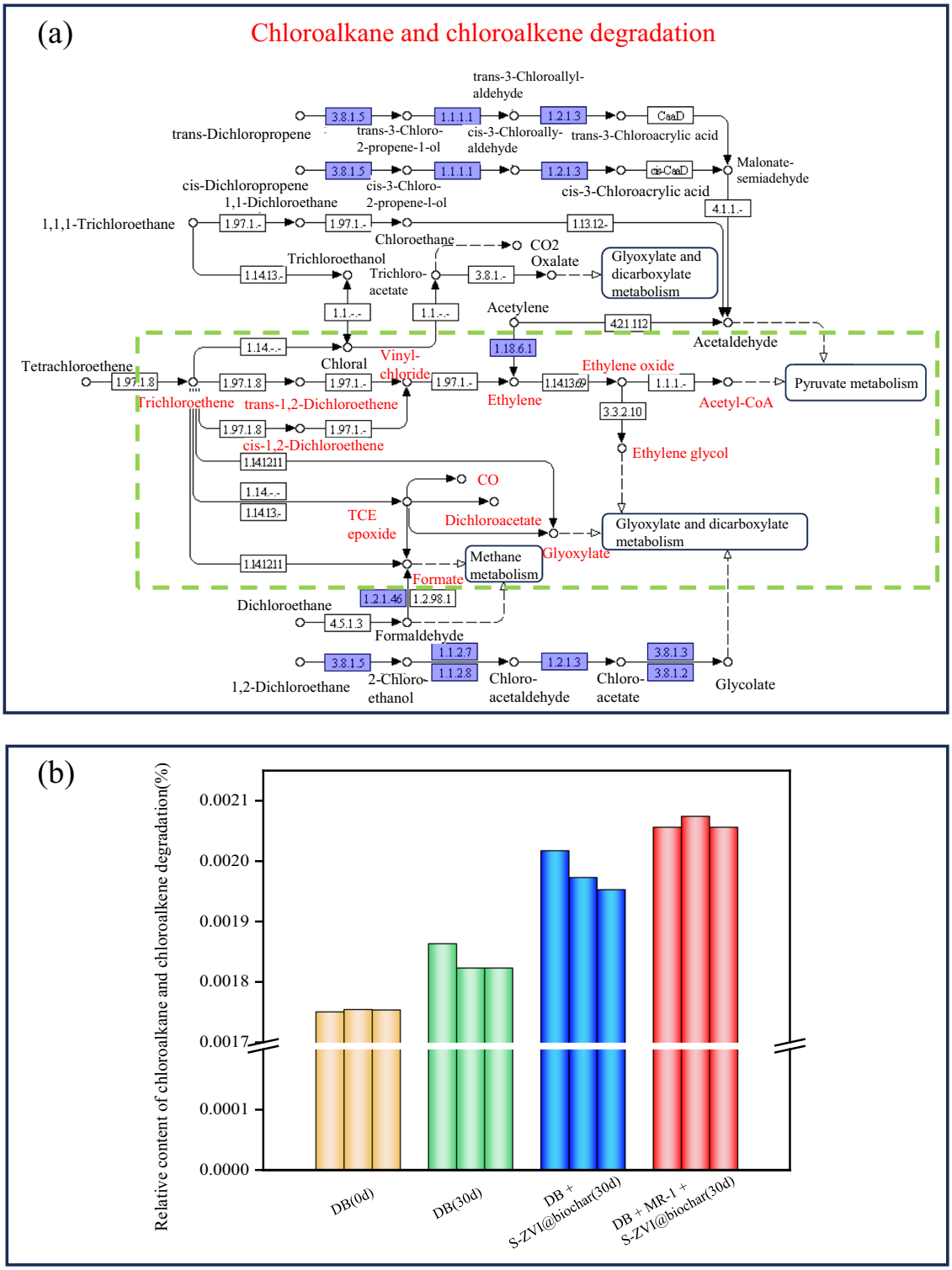

Fig. 9 | Genetic potential of microbial communities and relative proportions of chloroalkane and chloroalkene degradation processes to all life processes. a The predicted enzymes were mapped on chloroalkane and chloroalkene biodegradation pathways. Circles represent pollutants, boxes represent the enzymes used in the degradation pathway. Microorganisms have multiple pathways for dechlorinating chloroalkane and chloroalkene and have good potential for dechlorination. **b** Relative proportions of chloroalkane and chloroalkene degradation processes to all life processes in different systems. Both S-ZVI@biochar and MR-1 stimulate microbial communities to enhance their dechlorination processes.

reconverted back to Fe(III) after dechlorination of chlorinated organic matter, realizing the recycling of iron in the system, which has potential for sustainable remediation applications.

In this study, the dechlorination process and promoted mechanisms by the coupling of DB, MR-1 and S-ZVI@biochar were explained as follows: (1) The biochar in S-ZVI@biochar acted as a support for DB and MR-1, allowing microorganisms to grow rapidly on its surface. (2) The biochar in S-ZVI@biochar could adsorb TCE, which drew microorganisms, S-ZVI@biochar, and TCE closer, and facilitated electron transfer among them. Bio-dechlorination and chemical dechlorination were synchronized and

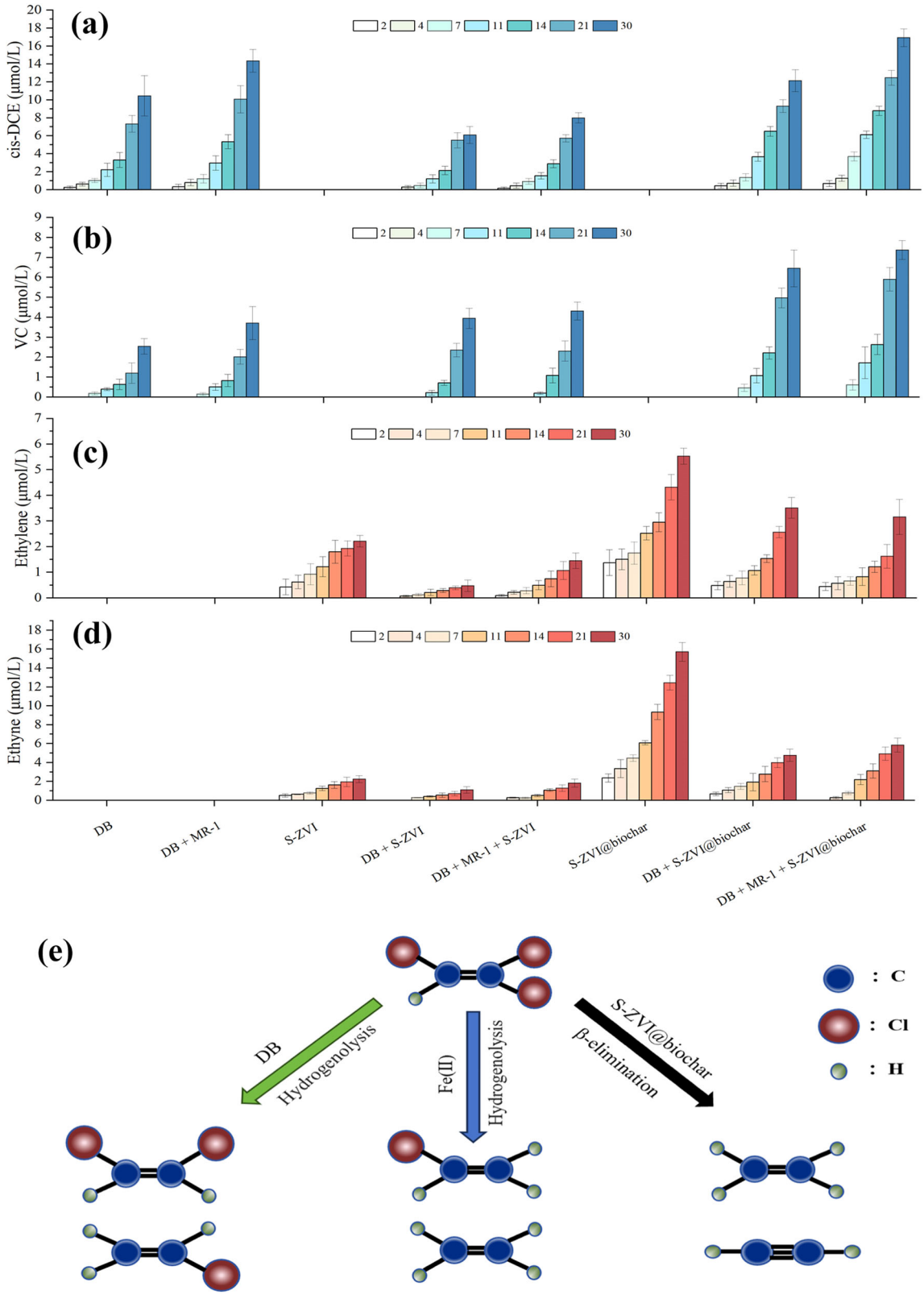

Fig. 10 | Dechlorination product content over time in different reaction systems. **a** The cis-DCE content over time in different reaction systems, and the DB + MR-1 + S-ZVI@biochar system produces more cis-DCE. **b** The VC content over time in different reaction systems, and the DB + MR-1 + S-ZVI@biochar system produces more VC. **c** The Ethylene content over time in different reaction systems, and the S-ZVI@biochar system produces more Ethylene. **d** The Ethyne content over time in different reaction systems, and the S-ZVI@biochar system produces more Ethyne. **e** Degradation pathways of TCE. Dechlorination of TCE through DB hydrogenolysis, β-elimination by S-ZVI@biochar, and hydrogenolysis by biogenic Fe(II).

enhanced. (3) S-ZVI@biochar degraded TCE by β-elimination (formation of an additional C-C bond with loss of two vicinal halogens) and hydrogenolysis (replacement of a halogen substituent by hydrogen). DB degraded TCE via hydrogenolysis. (4) The good electrical conductivity of biochar benefited the transfer of electrons generated by S-ZVI@biochar to DB and MR-1, and DB utilized the electrons for dechlorination of the electron acceptor TCE, while MR-1 utilized them to convert Fe(III) generated by the corrosion of S-ZVI@biochar into Fe(II), which continued to participate in the removal of TCE. (5) MR-1 consumed sodium acetate in the system to provide nutrients for DB and promote the growth of microorganisms with functions such as hydrogen production and dehalogenation.

This study is the first to construct a directed electron transfer channel between microorganisms and TCE by modifying S-ZVI with biochar. The modified S-ZVI@biochar showed good mobility and synergistic effects with microorganisms. Comparing the DB + MR-1 + S-ZVI system with the DB + MR-1 + S-ZVI@ biochar system, S-ZVI@biochar had a positive effect on both chemical remediation and bioremediation, significantly improving the overall removal performance of the system for TCE. The TCE removal of system DB + MR-1 + S-ZVI@biochar was 73.9% and 9.1% higher than system DB and S-ZVI@biochar, respectively. In the DB + MR-1 + S-ZVI@biochar system, hydrogen accumulation lagged behind the significant removal of TCE, verifying that dehalogenating microorganisms effectively utilized hydrogen. Based on SEM, XRD, and XPS data, the DB + MR-1 + S-ZVI@biochar system showed the addition of MR-1 increased the solid-phase Fe(II)/Fe(III) ratio from 0.4782 to 0.6690 in the DB + MR-1 + S-ZVI@-biochar system compared to the DB + S-ZVI@biochar system, suggesting that MR-1 can bioconvert Fe(III) to Fe(II) with dechlorination ability, thus cycling iron in the system. S-ZVI@biochar played a key role in linking the chemical dechlorination process with the biological dechlorination process. The electrons generated by S-ZVI@biochar were transferred to DB and TCE via biochar, and DB transferred electrons to TCE via biochar, which made biochar a promising option for in situ remediation of TCE linking the chemical materials with microorganisms.

Data availability

The datasets used and analysed during the current study available from the corresponding author on reasonable request. All applicable data is provided in the figures and tables of the manuscript.

Received: 5 April 2024; Accepted: 23 August 2024;
Published online: 31 August 2024

References

1. Zhao, X. et al. An overview of preparation and applications of stabilized zero-valent iron nanoparticles for soil and groundwater remediation. *Water Res.* **100**, 245–266 (2016).
2. Liu, H. et al. Electron efficiency of zero-valent iron for groundwater remediation and wastewater treatment. *Chem. Eng. J.* **215**, 90–95 (2013).
3. Gu, Y. et al. Mechanochemically Sulfidated Microscale Zero Valent Iron: Pathways, Kinetics, Mechanism, and Efficiency of Trichloroethylene Dechlorination. *Environ. Sci. Technol.* **51**, 12653–12662 (2017).
4. Tang, J. et al. Reductive dechlorination of trichloroethene by sulfided microscale zero-valent iron in fresh and saline groundwater: Reactivity, pathways, and selectivity. *Chemosphere* **340**, 139900–139900 (2023).
5. Maymo-Gatell, X. et al. Isolation of a bacterium that reductively dechlorinates tetrachloroethene to ethene. *Science* **276**, 1568–1571 (1997).
6. Chung, J., Krajmalnik-Brown, R. & Rittmann, B. E. Bioreduction of trichloroethene using a hydrogen-based membrane biofilm reactor. *Environ. Sci. Technol.* **42**, 477–483 (2008).
7. Tang, F. et al. Individual and combined effects of humic acid, bicarbonate and calcium on TCE removal kinetics, aging behavior and electron efficiency of mZVI particles. *Chem. Eng. J.* **324**, 324–335 (2017).
8. Noubactep, C. A critical review on the process of contaminant removal in Fe-0-H_2O systems. *Environ. Technol.* **29**, 909–920 (2008).
9. Yuan, M. et al. Coupling microscale zero-valent iron and autotrophic hydrogen-bacteria provides a sustainable remediation solution for trichloroethylene-contaminated groundwater: Mechanisms, regulation, and engineering implications. *Water Res.* **216**, 0043–1354 (2022).
10. Kocur, C. M. D. et al. Long-Term Field Study of Microbial Community and Dechlorinating Activity Following Carboxymethyl Cellulose-Stabilized Nanoscale Zero-Valent Iron Injection. *Environ. Sci. Technol.* **50**, 7658–7670 (2016).
11. de Guzman, G. T. N. et al. Presence of organohalide-respiring bacteria in and around a permeable reactive barrier at a trichloroethylene-contaminated Superfund site. *Environ. Pollut.* **243**, 766–776 (2018).
12. Rangan, S. M. et al. Synergistic Zerovalent Iron (Fe-0) and Microbiological Trichloroethene and Perchlorate Reductions Are Determined by the Concentration and Speciation of Fe. *Environ. Sci. Technol.* **54**, 14422–14431 (2020).
13. Rangan, S. M. et al. Decoupling Fe0 Application and Bioaugmentation in Space and Time Enables Microbial Reductive Dechlorination of Trichloroethene to Ethene: Evidence from Soil Columns. *Environ. Sci. Technol.* **57**, 4167–4179 (2023).
14. Zheng, Z. et al. Reductive dechlorination of hexachlorobenzene by Cu/Fe bimetal in the presence of nonionic surfactant. *J. Hazard. Mater.* **170**, 895–901 (2009).
15. Fan, P. et al. Coupled Effect of Sulfidation and Ferrous Dosing on Selenate Removal by Zerovalent Iron Under Aerobic Conditions. *Environ. Sci. Technol.* **53**, 14577–14585 (2019).
16. Li, T. et al. Phosphidation of microscale zero-valent iron (P-mZVI) for enhanced dechlorination of trichloroethylene. *J. Clean. Prod.* **386**, 135803 (2023).
17. Yan, Z. et al. Nonmetallic modified zero-valent iron for remediating halogenated organic compounds and heavy metals: A comprehensive review. *Environ. Sci. Ecotechnol.* **21**, 100417 (2024).
18. Liu, S. et al. Mechanism and Application of Nanoscale Zero-valent Iron and Modified Materials in Groundwater Remediation. *Environ. Sci. Technol.* **45**, 181–193 (2022).
19. Shi, Z. et al. Methods for characterizing the fate and effects of nano zerovalent iron during groundwater remediation. *J. Contaminant Hydrol.* **181**, 17–35 (2015).
20. Guo, J. et al. Sulfidation of zero-valent iron for enhanced reduction of chlorinated contaminants: A review on the reactivity, selectivity, and interference resistance. *Chem. Eng. J.* **477**, 147049 (2023).
21. Rajajayavel, S. R. C. & Ghoshal, S. Enhanced reductive dechlorination of trichloroethylene by sulfidated nanoscale zerovalent iron. *Water Res.* **78**, 144–153 (2015).
22. Huang, D. et al. Mechanochemically Sulfidated Zero Valent Iron as an Efficient Fenton-like Catalyst for Degradation of Organic Contaminants. *Acta Chim. Sin.* **75**, 866–872 (2017).
23. Kim, E.-J. et al. Facile Synthesis and Characterization of Fe/FeS Nanoparticles for Environmental Applications. *Acs Appl. Mater. Interfaces* **3**, 1457–1462 (2011).
24. Dong, H. et al. Factors influencing degradation of trichloroethylene by sulfide-modified nanoscale zero-valent iron in aqueous solution. *Water Res.* **135**, 1–10 (2018).
25. Li, D. et al. Abiotic transformation of hexabromocyclododecane by sulfidated nanoscale zerovalent iron: Kinetics, mechanism and influencing factors. *Abstr. Pap. Am. Chem. Soc.* **253**, 0065–7727 (2017).
26. Gong, L. et al. Coincorporation of N and S into Zero-Valent Iron to Enhance TCE Dechlorination: Kinetics, Electron Efficiency, and Dechlorination Capacity. *Environ. Sci. Technol.* **55**, 16088–16098 (2021).

27. Hou, J. et al. The role of nitrate in simultaneous removal of nitrate and trichloroethylene by sulfidated zero-valent Iron. *Sci. Total Environ.* **829**, 154304 (2022).
28. Yang, Z. et al. Re-activation of aged-ZVI by iron-reducing bacterium Shewanella putrefaciens for enhanced reductive dechlorination of trichloroethylene. *J. Chem. Technol. Biotechnol.* **92**, 2642–2649 (2017).
29. Li, Y. et al. Addition of Shewanella oneidensis MR-1 to the Dehalococcoides-containing culture enhances the trichloroethene dechlorination. *Environ. Int.* **133**, 105245 (2019).
30. Li, F. B. et al. Enhanced reductive dechlorination of DDT in an anaerobic system of dissimilatory iron-reducing bacteria and iron oxide. *Environ. Pollut.* **158**, 1733–1740 (2010).
31. Nie, Z. et al. Biogenic FeS promotes dechlorination and thus de-cytotoxity of trichloroethylene. *Bioprocess Biosyst. Eng.* **43**, 1791–1800 (2020).
32. Shin, H. Y., Singhal, N. & Park, J. W. Regeneration of iron for trichloroethylene reduction by Shewanella alga BrY. *Chemosphere* **68**, 1129–1134 (2007).
33. Royer, R. A. et al. Enhancement of Biological Reduction of Hematite by Electron Shuttling and Fe(II) Complexation. *Environ. Sci. Technol.* **36**, 1939–1946 (2002).
34. Wang, X. et al. Electron competition and electron selectivity in abiotic, biotic, and coupled systems for dechlorinating chlorinated aliphatic hydrocarbons in groundwater: A review. *Water Res.* **183**, 0043–1354 (2020).
35. Lyu, H. et al. Functional materials contributing to the removal of chlorinated hydrocarbons from soil and groundwater: Classification and intrinsic chemical-biological removal mechanisms. *Sci. Total Environ.* **879**, 163011 (2023).
36. Chen, Z. et al. Enhancing the removal of chlorinated hydrocarbons from groundwater using a new BL5 microorganism with functional CS@ZVI materials. *J. Water Process Eng.* **57**, 104699 (2024).
37. Liu, Y. et al. Enhanced trichloroethylene biodegradation: Roles of biochar-microbial collaboration beyond adsorption. *Sci. Total Environ.* **792**, 148451 (2021).
38. Semerad, J. et al. Discovering the potential of an nZVI-biochar composite as a material for the nanobioremediation of chlorinated solvents in groundwater: Degradation efficiency and effect on resident microorganisms. *Chemosphere* **281**, 130915 (2021).
39. Shah, V. et al. Taxonomic Profiling and Metagenome Analysis of a Microbial Community from a Habitat Contaminated with Industrial Discharges. *Microb. Ecol.* **66**, 533–550 (2013).
40. Handelsman, J. Metagenomics: Application of genomics to uncultured microorganisms. *Microbiol. Mol. Biol. Rev.* **68**, 669 (2004).
41. Löffler, F. E., Sanford, R. A., and Ritalahti, K. M., Enrichment, cultivation, and detection of reductively dechlorinating bacteria, In *Environmental Microbiology*, Leadbetter, J. R., Editor. p. 77-111 (2005).
42. Cai, S. et al. Sulfidation of Zero-Valent Iron by Direct Reaction with Elemental Sulfur in Water: Efficiencies, Mechanism, and Dechlorination of Trichloroethylene. *Environ. Sci. Technol.* **55**, 645–654 (2021).
43. Ri, C. et al. Ball-milled Fe^0/FeS_2 enhanced interaction of Shewanella oneidensis MR-1 with anaerobic microbial community: Impact on 2,4-dichloronitrobenzene reduction and methane yield. *Chem. Eng. J.* **452**, 139086 (2023).
44. Bowman, K. S., Rainey, F. A. & Moe, W. M. Production of hydrogen by Clostridium species in the presence of chlorinated solvents. *Fems Microbiol. Lett.* **290**, 188–194 (2009).
45. Perez-Rangel, M. et al. The duo Clostridium and Lactobacillus linked to hydrogen production from a lignocellulosic substrate. *Water Sci. Technol.* **83**, 186 (2021).
46. Lin, W. H. et al. Growth inhibition of methanogens for the enhancement of TCE dechlorination. *Sci. Total Environ.* **787**, 147648 (2021).
47. Elbeshbishy, E. et al. A critical review on inhibition of dark biohydrogen fermentation. *Renew. Sustain. Energy Rev.* **79**, 656–668 (2017).
48. Wong, Y. M., Wu, T. Y. & Juan, J. C. A review of sustainable hydrogen production using seed sludge via dark fermentation. *Renew. Sustain. Energy Rev.* **34**, 471–482 (2014).
49. Wang, J. & Wan, W. Factors influencing fermentative hydrogen production: A review. *Int. J. Hydrog. Energy* **34**, 799–811 (2009).
50. Dos Passos, V. F. et al. Hydrogen and electrical energy co-generation by a cooperative fermentation system comprising Clostridium and microbial fuel cell inoculated with port drainage sediment. *Bioresour. Technol.* **277**, 94–103 (2019).
51. Wang, Y. et al. The role of Fe_3O_4@biochar as electron shuttle in enhancing the biodegradation of gaseous para-xylene by aerobic surfactant secreted strains. *J. Hazard. Mater.* **438**, 129475 (2022).
52. Kim, H., Ahn, D. & Annable, M. D. Enhanced removal of VOCs from aquifers during air sparging using thickeners and surfactants: Bench-scale experiments. *J. Contaminant Hydrol.* **184**, 25–34 (2016).
53. Ji, J. et al. Review of biodegradation of sulfonamide antibiotics influenced by dissolved organic matter and iron oxides. *J. Environ. Chem. Eng.* **11**, 111020 (2023).
54. Zhong, H. et al. Application of dissimilatory iron-reducing bacteria for the remediation of soil and water polluted with chlorinated organic compounds: Progress, mechanisms, and directions. *Chemosphere* **352**, 141505–141505 (2024).
55. Liang, J. et al. Reduction of nitrobenzene in ground water by the combination of zero valent iron and anaerobic microorganism. *Chin. J. Environ. Eng.* **6**, 2512–2516 (2012).
56. Brookshaw, D. R. et al. Redox Interactions Between Cr(VI) and Fe(II) in Bioreduced Biotite and Chlorite. *Environ. Sci. Technol.* **48**, 11337–11342 (2014).
57. Ghorbanzadeh, N. et al. Removal of chromium Cr(VI) from contaminated solutions by using biogenic ferrous iron in bioreduced minerals. *Geosyst. Eng.* **17**, 95–103 (2014).
58. Kong, L.-L., Liu, W.-T., and Zhou, Q.-X., Biochar: An Effective Amendment for Remediating Contaminated Soil, In *Reviews of Environmental Contamination and Toxicology*, Vol 228, Whitacre, D. M. Editor. p. 83-99. (2014)
59. Zhou, S. et al. Enhanced Cr(VI) removal by biochar-loaded zero-valent iron coupled with weak magnetic field. *J. Water Process Eng.* **47**, 102732 (2022).
60. Li, Y. et al. Strategy and mechanisms of sulfamethoxazole removal from aqueous systems by single and combined Shewanella oneidensis MR-1 and nanoscale zero-valent iron-enriched biochar. *Sci. Total Environ.* **883**, 163676 (2023).
61. Jie, C., Yin, C. H. U. & Youbin, S. I. Dissimilatory Fe(III)reduction by Shewanclla oneidensis MR-1 and impact factors. *J. Anhui Agric. Univ.* **38**, 554–558 (2011).
62. Bae, Y. et al. Transformation impacts of dissolved and solid phase Fe(II) on trichloroethylene (TCE) reduction in an iron-reducing bacteria (IRB) mixed column system: A mathematical model. *Water Res.* **46**, 6391–6398 (2012).
63. Maithreepala, R. A. & Doong, R. A. Synergistic effect of copper ion on the reductive dechlorination of carbon tetrachloride by surface-bound Fe(II) associated with goethite. *Environ. Sci. Technol.* **38**, 260–268 (2004).
64. Zhang, X. et al. Biochar-Mediated Anaerobic Oxidation of Methane. *Environ. Sci. Technol.* **53**, 6660–6668 (2019).
65. Yamashita, T. & Hayes, P. Analysis of XPS spectra of Fe^{2+} and Fe^{3+} ions in oxide materials. *Appl. Surf. Sci.* **254**, 2441–2449 (2008).
66. Wang, B. et al. Influence of different co-contaminants on trichloroethylene removal by sulfide-modified nanoscale zero-valent iron. *Chem. Eng. J.* **381**, 122773 (2020).
67. Gao, F. et al. Enhanced reductive degradation of tetrabromobisphenol A by biochar supported sulfidated nanoscale zero-valent iron: Selectivity and core reactivity. *Appl. Catal. B-Environ.* **324**, 122246 (2023).

68. Liang, L. et al. Effects of magnetic field on selenite removal by sulfidated zero valent iron under aerobic conditions. *Sci. Total Environ.* **831**, 154755 (2022).
69. Cheng, Z. et al. Removal of antimonite (Sb(III)) from aqueous solution using a magnetic iron-modified carbon nanotubes (CNTs) composite: Experimental observations and governing mechanisms. *Chemosphere* **288**, 132581 (2022).
70. Uchimiya, M. & Stone, A. T. Redox reactions between iron and quinones: Thermodynamic constraints. *Geochimica Et. Cosmochimica Acta* **70**, 1388–1401 (2006).
71. Xiong, L. et al. Shewanella oneidensis MR-1 for enhanced the reactivity of FA-stabilized nZVI toward Cr(VI) removal. *Sep. Purif. Technol.* **305**, 122542 (2023).
72. Mullet, M., Guillemin, Y. & Ruby, C. Oxidation and deprotonation of synthetic FeII-FeIII (oxy)hydroxycarbonate Green Rust:: An X-ray photoelectron study. *J. Solid State Chem.* **181**, 81–89 (2008).
73. Islam, M. N. et al. Superoxide dismutase: an updated review on its health benefits and industrial applications. *Crit. Rev. Food Sci. Nutr.* **62**, 7282–7300 (2022).
74. del Rio, L. A. & Lopez-Huertas, E. ROS Generation in Peroxisomes and its Role in Cell Signaling. *Plant Cell Physiol.* **57**, 1364–1376 (2016).
75. Lee, S.-S. & 박우정 The Biological Degradation of High Concentration of Trichloroethylene (TCE) by Delftia acidovornas EK2. *Korean J. Microbiol.* **46**, 183–191 (2010).
76. Lee, W.-S. et al. Serial degradation of perchloroethylene by Delftia sp N6 after dechlorination using Fenton's reagent. *J. Microbiol. Biotechnol.* **16**, 1734–1739 (2006).
77. Lu, Q. et al. Combined removal of a BTEX, TCE, and cis-DCE mixture using Pseudomonas sp immobilized on scrap tyres. *Environ. Sci. Pollut. Res.* **22**, 14043–14049 (2015).
78. Baskaran, D. & Rajamanickam, R. Aerobic biodegradation of trichloroethylene by consortium microorganism from turkey litter compost. *J. Environ. Chem. Eng.* **7**, 103260 (2019).
79. Li, J. et al. Coupling of biostimulation and bioaugmentation for enhanced bioremoval of chloroethylenes and BTEX from clayey soil. *Ecotoxicology* **30**, 1446–1453 (2021).
80. Shanbhogue, S. S. et al. Trichloroethene removal by separately encapsulated and co-encapsulated bacterial degraders and nanoscale zero-valent iron. *Int. Biodeterior. Biodegrad.* **125**, 269–276 (2017).
81. Kao, C.-M. et al. The change of microbial community from chlorinated solvent-contaminated groundwater after biostimulation using the metagenome analysis. *J. Hazard. Mater.* **302**, 144–150 (2016).
82. Wang, Q. et al. Insitu remediation of Cr(VI) contaminated groundwater by ZVI-PRB and the corresponding in digenous microbial community responses: a field-scale study. *Sci. Total Environ.* **805**, 150260 (2022).
83. Mi, J.-X. et al. Comparative analysis of the gut microbiota of wild wintering whooper swans (Cygnus Cygnus), captive black swans (Cygnus Atratus), and mute swans (Cygnus Olor) in Sanmenxia Swan National Wetland Park of China. *Environ. Sci. Pollut. Res.* **30**, 93731–93743 (2023).
84. Basu, A., Manna, S. & Sil, A. K. A new electro-active bacterium, Paraclostridium sp. AKS46, converts waste efficiently into electricity in microbial fuel cell. *Chem. Eng. J.* **475**, 145626 (2023).
85. Chen, J. et al. Insight into the enhancement effect of humic acid on microbial degradation of triclosan in anaerobic sediments. *J. Hazard. Mater.* **461**, 132549 (2024).
86. Yeap, C. S. Y. et al. Dissolved iron released from nanoscale zero-valent iron (nZVI) activates the defense system in bacterium Pseudomonas putida, leading to high tolerance to oxidative stress. *J. Hazard. Mater.* **439**, 129627 (2022).
87. Wei, X. et al. Reductive debromination of decabromodiphenyl ether by iron sulfide-coated nanoscale zerovalent iron: mechanistic insights from Fe(II) dissolution and solvent kinetic isotope effects. *Environ. Pollut.* **253**, 161–170 (2019).
88. Wei, X. et al. Reactive oxygen species generated in iron sulfide mediated advanced oxidation systems: A critical review of mechanisms and implications for geochemistry and environmental remediation. *J. Environ. Chem. Eng.* **10**, 108841 (2022).
89. Enache, T. A. & Oliveira-Brett, A. M. Phenol and para-substituted phenols electrochemical oxidation pathways. *J. Electroanal. Chem.* **655**, 9–16 (2011).
90. Fan, X. et al. Reversible redox reaction on the oxygen-containing functional groups of an electrochemically modified graphite electrode for the pseudo-capacitance. *J. Mater. Chem.* **21**, 18753–18760 (2011).
91. Saquing, J. M., Yu, Y.-H. & Chiu, P. C. Wood-Derived Black Carbon (Biochar) as a Microbial Electron Donor and Acceptor. *Environ. Sci. Technol. Lett.* **3**, 62–66 (2016).
92. Chacon, F. J. et al. Understanding, measuring and tuning the electrochemical properties of biochar for environmental applications. *Rev. Environ. Sci. Bio-Technol.* **16**, 695–715 (2017).
93. Palansooriya, K. N. et al. Response of microbial communities to biochar-amended soils: a critical review. *Biochar* **1**, 3–22 (2019).
94. Yu, L. et al. Biochar as Electron Acceptor for Microbial Extracellular Respiration. *Geomicrobiol. J.* **33**, 530–536 (2016).
95. Chen, J. et al. Biochar accelerates microbial reductive debromination of 2,2 ',4,4 '-tetrabromodiphenyl ether (BDE-47) in anaerobic mangrove sediments. *J. Hazard. Mater.* **341**, 177–186 (2018).
96. Yu, L. et al. Biochar as an electron shuttle for reductive dechlorination of pentachlorophenol by Geobacter sulfurreducens. *Sci. Rep.* **5**, 16221 (2015).
97. Tong, H. et al. Biochar enhances the microbial and chemical transformation of pentachlorophenol in paddy soil. *Soil Biol. Biochem.* **70**, 142–150 (2014).
98. Kouzuma, A., Kato, S. & Watanabe, K. Microbial interspecies interactions: recent findings in syntrophic consortia. *Front. Microbiol.* **6**, 00477 (2015).

Acknowledgements

The authors gratefully acknowledge financial support for this work from the (1) Science Fund for Distinguished Young Scholars of Tianjin (23JCJQJC00120); (2) Science Fund for Distinguished Young Scholars of Hebei Province (D2023202007); (3) National Natural Science Foundation of China (22106037, 42177218), (4) the Natural Science Foundation of Hebei Province (B2024202024), and (5) the S&T Program of Hebei (21374204D, 22374206D).

Author contributions

Honghong Lyu: conceived and designed the manuscript, drafted the manuscript, reviewed and polished the article, and funded the acquisition. Hua Zhong: drafted the manuscript, methodology and software. Zhilian Li: revised the manuscript, methodology and software. Zhiqiang Wang: methodology and software. Zhineng Wu: reviewed and polished the article, funding acquisition. Jingchun Tang: reviewed and polished the article.

Competing interests

The authors declare no competing interests.

Additional information

Supplementary information The online version contains supplementary material available at https://doi.org/10.1038/s41545-024-00376-9.

Correspondence and requests for materials should be addressed to Honghong Lyu, Zhineng Wu or Jingchun Tang.